Utrecht University

MASTER THESIS

A mathematical model of vegetation-topography feedbacks and their impact on the resilience of arid ecosystems

Author:
Tri J. M. SAMBAS

Supervisors:
dr. P. A. ZEGELING
K. SITEUR, Ph.D
prof. dr. J. VAN DE KOPPEL

Examiner:
prof. dr. ir. M. RIETKERK

A thesis submitted in fulfillment of the requirements for the degree of Master of Science in MATHEMATICS

at the

Department of Mathematics

combined with an internship at

January 9, 2019

Acknowledgements

This thesis is combined with an internship at NIOZ, Royal Netherlands Institute for Sea Research, in Yerseke, from June 2018 until November 2018. I would like to begin by thanking my two supervisors from NIOZ, Koen Siteur, Ph.D. and prof. dr. Johan van de Koppel and my project supervisor from Utrecht University, dr. Paul Zegeling for their fruitful discussion and insightful feedback during the process. I would like to thank prof. dr. ir. Max Rietkerk from Utrecht University for willing to be my second examiner of the thesis. Next, I would also like to thank my colleagues at NIOZ for making a move to a small village in Zeeland easy by doing a lot of fun activities.

Further, I would like to thank my scholarship provider, Indonesian Endowment Fund for Education (LPDP) for giving me a chance for studying abroad. After that, I would like to thank my biggest supporting system, Mamah, Papah, Aa, Teteh dan Sucha. Finally, for all of my Indonesian and International friends in Utrecht, thank you very much for your support.

UTRECHT UNIVERSITY

Abstract

Faculty of Science
Department of Mathematics

Master of Science in MATHEMATICS

A mathematical model of vegetation-topography feedbacks and their impact on the resilience of arid ecosystems

by Tri J. M. SAMBAS

Vegetation in arid ecosystems is a well-known example of self-organized spatial patterns. The pattern of vegetation bands interspersed with bare soil is explained as a result of positive feedback between infiltration and vegetation. In gently sloped landscapes, vegetation patterns appear as vegetation bands which are perpendicular to the direction of the slope. Moreover, it is widely observed that vegetation bands are found to be arced and convex up-slope. Previous studies suggest that the underlying topography plays a role in shaping the bands as the straight bands are changing to arced when it grows on top of valley-like landscapes. Although it is clear that topography affects the shape of vegetation patterns, it is yet unknown how feedbacks between vegetation and topography influence the resilience of self-organized patterns in arid ecosystems.

In this study, we develop a mathematical model based on the interaction between hydrodynamics, vegetation, and topography. We start with modifying the surface water model by Rietkerk et al., 2002 into the shallow water equations and adding a topography dynamics to allow soil erosion. Additionally, we simulate the effect of environmental changes, for example, rainfall pattern to the resilience of vegetation in the presence of topography evolution. The simulation results show that a long dry period could trigger channel formation which then causes an accumulation of water. We also found that as the amount of water increasing in the channels, vegetation begins to inhabit the channels and prevent soil erosion to deepen the channels further. Therefore, we argue that the topographic depression and channels could increase the resilience of vegetation bands in dealing with harsh conditions, by helping the vegetation in concentrating and harvesting water. Finally, our findings suggest that these arced band patterns could be an indicator of a system that is recovering.

Keywords: arid ecosystems, self-organization, spatial patterns, Turing pattern, shallow water equations, geomorphology.

Contents

List of Figures

List of Tables

For my family, friends, and whoever has supported me during these two years of study in the Netherlands …

Chapter 1

Introduction

Arid ecosystems are found on nearly every continent, i.e., Africa, Asia, America, and Australia. This ecosystem is characterized by a limited amount of water found in the area due to lack of precipitation and also classified as drylands (details can be found in Figure 1.1). Same as the other drylands system, arid ecosystems are prone to desertification. Overgrazing and changes in land use by human activities could pose a threat to the ecosystems (Adeel et al., 2005, Gowda, Iams, and Silber, 2018). Moreover, climate change could also play a role in land degradation due to the change in rainfall patterns (Hendrix and Salehyan, 2012). Therefore, research regarding the evolution of composition in ecosystems, especially vegetation, are needed to assess the potential threats in ecosystem management.

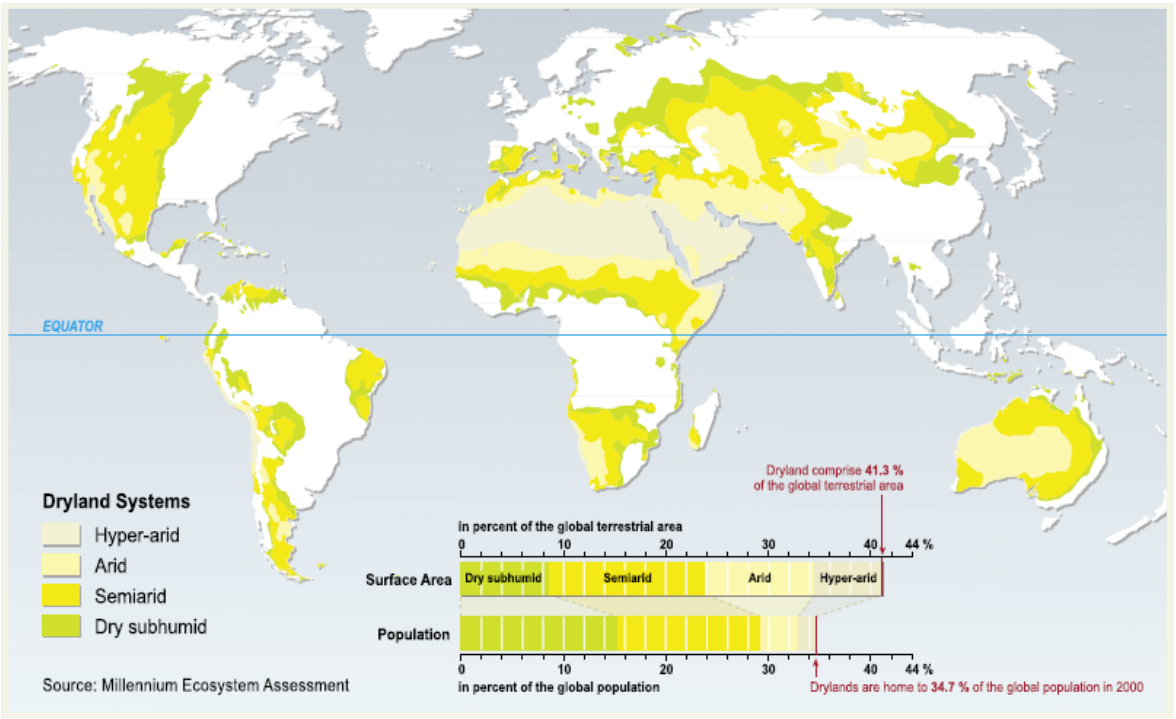

FIGURE 1.1: The classification and distribution of dryland systems in the earth surface, starting from dry sub-humid to hyper-arid (desert). This image was taken from Adeel et al., 2005. Dryland systems contribute to about 41 % land mass of earth surface and are home to around 35% of the population in the world.

Many arid ecosystems, especially those are untouched by human, exhibit spatial vegetation patterns. The patterns consist of bare soil areas alternating with vegetation patches. The examples of these patterns are spots, gap, labyrinth, and regular bands. The first three examples are mostly found in flat landscapes whereas the lasts are found in gently sloping

landscapes (Couteron and Lejeune, 2001, Rietkerk et al., 2002, Deblauwe et al., 2011, Bastiaansen et al., 2018). It has been suggested by many (Klausmeier, 1999, Rietkerk et al., 2002, Hardenberg et al., 2001, Gilad et al., 2004) that these patterns can emerge due to positive feedbacks between infiltration and vegetation. A higher infiltration rate in vegetated areas than in bare soil areas leads the net displacement of water from run-off areas into vegetation patches. This process of making large-scale spatial patterns from random distributed initial conditions through local interactions is usually called spatial self-organization (Rietkerk and Koppel, 2008).

Mathematical modeling has become a well-known tool to simulate spatial vegetation patterns and assess potential threats to ecosystems health. In a study by Klausmeier, 1999, they built a simple mathematical model which could reproduce a regular stripes vegetation pattern found in arid and semi-arid ecosystems. Furthermore, HilleRisLambers et al., 2001, which was then extended by Rietkerk et al., 2002, expanded water modeling as two dependent variables, i.e., surface water and soil water which could recreate the whole range of distinctive patterns in arid ecosystems. In other previous studies (Scheffer et al., 2001, Rietkerk et al., 2004), they indicate a mechanism of patterns transformation from one to another by reducing and increasing resource input which could be an indicator of a catastrophic shift from a vegetated to a degraded state. However, their models have not taken into account the influence of topography variation on vegetation patterning. Meanwhile, the studies by Macfadyen, 1950 and Deblauwe et al., 2011 suggest the importance of topography role in shaping vegetation pattern. In an aerial photograph, Macfadyen, 1950 shows two different vegetation conditions sitting side by side; one is a gently sloped landscape with vegetation banded patterns while the other one is a highly eroded landscape with less vegetation. Correspondingly, the study by Deblauwe et al., 2011 reveals that vegetation bands are only found in topography with a gradient between 0.25 - 1%. These two findings suggest that topography plays an important role in influencing the resilience of arid ecosystems. Therefore, it is essential to include the effect of topography variation into mathematical modeling of arid ecosystems.

Several previous studies have investigated the influence of topography variation in vegetation patterning by using extended models, but its impact on the resilience remains unexplored. Gandhi et al., 2018 extended the Klausmeier model to take the non-uniformity of underlying topography into account. The results show that vegetation "arced" bands are related to the curvature of valley-like landscapes. Saco, Willgoose, and Hancock, 2007, which later extended by the second paper Saco and Moreno-De Las Heras, 2013, were the first to introduce topography dynamics coupled with vegetation and hydrodynamics in arid ecosystems. The studies found that bumpy landscapes, which are seen in Australia, are a result of feedbacks between erosion and vegetation. Additionally, they indicate abiotic parameters (i.e., slope steepness, soil erodibility, and soil dispersion) impact on the biotic (i.e., vegetation patterning) which results in vegetation bands breaking up into stripes. However, they have not considered vegetation patterns responses to environmental changes, such as the change of rainfall pattern in which dry areas become drier while wet areas become wetter (Hendrix and Salehyan, 2012). Heterogeneous topographic conditions may alter the vegetation responses to the environmental changes. For example, topographic depressions, which are related to vegetation "arced" bands, might have a crucial role in low rainfall conditions since they form ponds of temporary water supply after rains (Macfadyen, 1950). Therefore, the interaction between vegetation and topography feedbacks give rise to further investigations.

In this study, we try to explain the observations done by Macfadyen, 1950 and Deblauwe et al., 2011. Based on the remote sensing data, vegetation bands only appear on gently sloped terrains. However, vegetation bands are observed side by side to a highly eroded landscape which has much less dense vegetation as shown in the photos of Macfadyen,

1950 (see Figure 1.2). The first finding suggests that vegetation bands maintain a relatively flat gradient while the second suggests that within the same conditions (i.e., rainfall pattern, soil composition), the two vegetation conditions with related landscapes are alternating to each other. In other words, in the first observation, negative feedbacks between vegetation and topography preserve the slope gradient whereas the second observation suggests that positive feedbacks can dominate the system which then generate a highly eroded landscape. Therefore, these observations indicate that feedbacks between vegetation and topography could control the resilience of arid ecosystems.

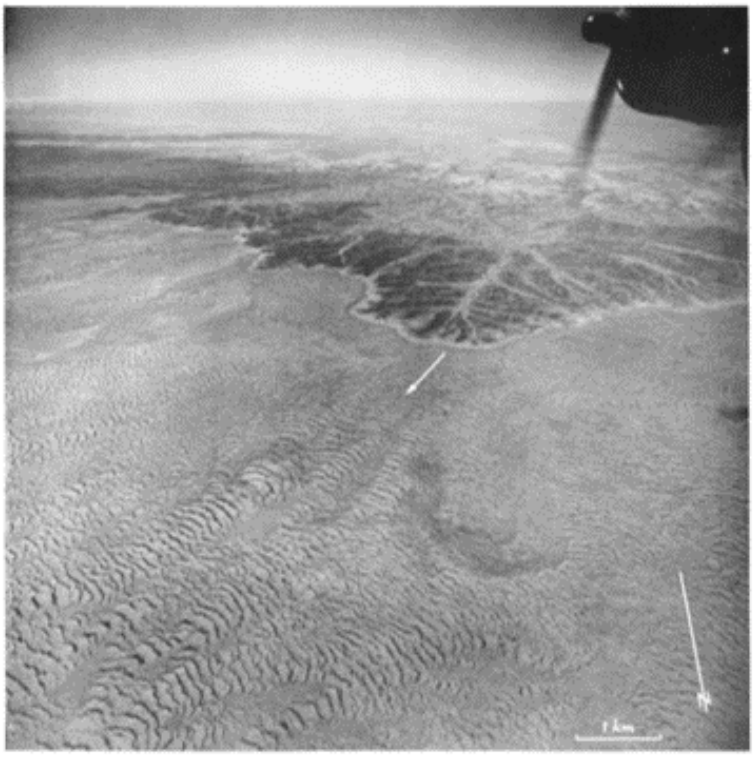

FIGURE 1.2: An aerial photograph of vegetation bands (foreground) and a highly eroded landscape (background) in a observational study by Macfadyen, 1950. The arrow represents the direction of the slope. Both conditions appear to be located side by side.

1.1 Hypotheses and Research Questions

Here we provide a complete explanation of two competing hypotheses which could explain the emergence of these two observed conditions. The hypotheses can be described as follows,

- Negative feedback hypothesis: Channels or topographic depressions concentrate water from rains thereby facilitating the growth of vegetation in the channels which prevent further erosion of the channels. Therefore, shallow depressions and channels induce an establishment of vegetation "arced" bands. Furthermore, the positive response from the channels to the vegetation growth could increase the resilience of the ecosystem against environmental changes. The illustration of this hypothesis can be found in Figure 1.3a.

- Positive feedback hypothesis: Deeper channels or topographic depressions concentrate more water thereby increasing water flow velocity. Because of the higher flow

velocity in the channels than the one goes to vegetation patches, it allows a "competition" between the vegetation and the channels in collecting water. The increased "competition" could lead to decreased vegetation density, due to the low water level on the ridges, and increased erosion rates on the valleys leading to deeper channels. Furthermore, the negative response from the channels to the vegetation growth could decrease the resilience of the ecosystem. The illustration of this hypothesis can be found in Figure 1.3b. Additionally, we can see that the highly eroded landscape is present next to vegetation banded patterns suggesting alternative stable ecosystem states and the potential for irreversible ecosystem degradation.

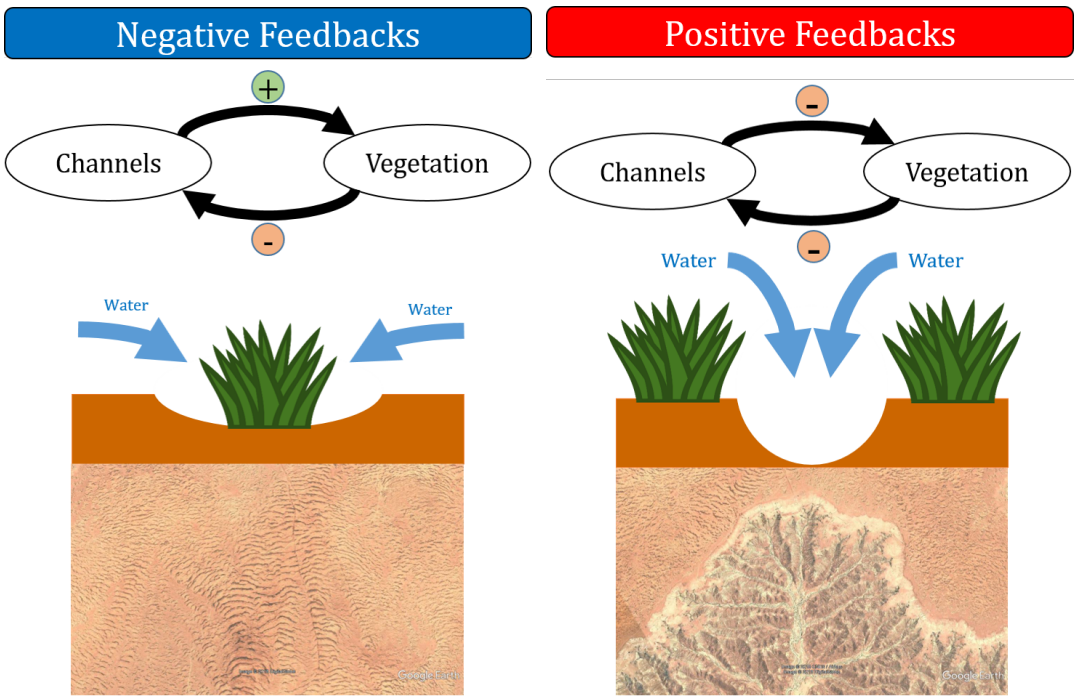

(A) Negative feedback hypothesis (B) Positive feedback hypothesis

FIGURE 1.3: The illustrations of negative and positive feedback hypotheses which explain vegetation "arced" banded patterns and "feather" patterns. Modern images are taken from the Google Earth Pro **(A)** in coordinates (9°19′55.52" N 48°45′25.68" E) and **(B)** in coordinates (9°17′11.10" N 48°43′25.72" E).

In this study, we want to investigate the implications of the interaction between biological processes that generate spatial vegetation patterns and morphological processes that determine soil erosion, to the resilience of arid ecosystems. In particular, we would like to address these two questions,

- Which biogeomorphic feedback dominates when it comes to the present vegetation "arced" bands and highly eroded landscapes?
- How do these feedbacks influence the stability/resilience of the ecosystem against environmental changes?

1.2 Aims

Our aims in this study can be described as follows,

- First, we would like to build a mathematical model which couples hydrodynamics, vegetation, and topography dynamics in arid ecosystems.
- Second, we want to investigate the influence of topography dynamics on the vegetation patterns and vice versa by using numerical simulations. In particular, we are interested in the evolution of vegetation patterns along with topography development.
- Third, we would like to analyze the impact of climate change, i.e., decreasing or increasing rainfall intensity, on the resilience of arid ecosystems.

1.3 Outline

In this study, we start with describing an established arid vegetation ecosystem modeling in Rietkerk et al., 2002 then modifying the surface water modeling to allow non-uniform water flow. Besides, we also add a topography dynamics to take the landscape formation into account. Furthermore, we include essential feedbacks between hydrodynamics, vegetation, and topography dynamics. Then, we use a numerical method to obtain the approximated solutions. Finally, we investigate the vegetation-topography relationship and its implication to the ecosystem resilience by using the proposed model.

The thesis organization is arranged as follows; in chapter 2, we would like to introduce the proposed model, numerical methods, and model analysis. In the proposed model, we provide descriptions of each model dynamics and a modeling scheme. For the numerical methods, we introduce the finite difference method to solve the system numerically. After that, to analyze the model results, we use the spectral analysis method and the continuation method. At the end of the chapter, we also would like to direct the reader to the initial setups of the numerical simulations. In chapter 3, we present the simulation results and analysis. Further elaboration of the results will be given in the discussion in chapter 4.

Chapter 2

Material and Methods

In this chapter, we are going to explain how vegetation, infiltration, and erosion feedbacks in arid ecosystems can be described as a set of mathematical expressions. After that, we will explain a numerical method called finite difference method to solve the equations numerically. In the end of the chapter, we would like to introduce two mathematical tools to analyze simulation results. Furthermore, we will also introduce three scenarios to mimic environmental changes.

2.1 Model Descriptions

Previous study by Rietkerk et al., 2002 has provided a basic model to explain the emergence of regular spatial patterns which are found in arid ecosystems. The model included positive feedback between infiltration and vegetation that influence water redistribution (see Figure 2.1). Water flow is assumed to be uniform, flat, and one-directional flow. Nevertheless, one of the keys to topographic variation in arid ecosystems is non-uniform water flow which allow an accumulation of water. Thus, we modify the surface water modeling by replacing the equation dynamics into shallow water equations to favor the non-uniform flow.

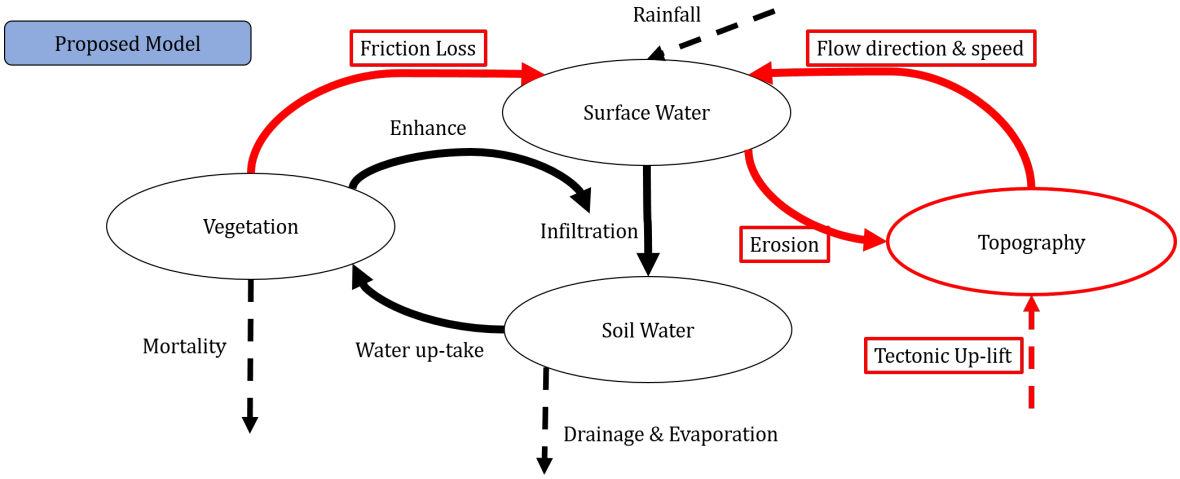

FIGURE 2.1: A conceptual model of arid ecosystem showing the interaction between vegetation, water, and topography dynamics. Black arrows are positive feedbacks to allow regular spatial patterns in arid ecosystems (study by Rietkerk et al., 2002) while red arrows represent the proposed feedbacks and a new proposed dynamic in this study.

Shallow water equations can generate non-uniform water flow via pressure differences and convective accelerations on x and y directions. Pressure differences, which come from

different height in water level, lead to varying local flow accelerations in the system. Meanwhile, convective accelerations allow increasing or decreasing flow speed which depend on underlying topography whether entering narrowing or opening, respectively. Both of them play a major role in creating non-uniform flow in fluid dynamics.

Non-uniform water flows induce topographic variations through soil erosion. As the water flow speed increases through narrow surfaces, soil erosion begin to take place. The erosion rates in narrow surfaces are higher compared to flat surfaces due to flow speed differences. Therefore, the narrow surfaces will get deeper through continuous soil erosion whereas the flat surfaces are barely eroded. The whole process of creating topographic variation is proposed to be called channelization process.

As the channelization process begins, topography is changing over time and give positive feedback to water flow. The change in topography will cause a redirection of water flow and an adjustment to the flow velocity. Channels divert flow directions from spreading out into concentrated and cause an accumulation of water. The accumulation of water induces pressure differences thereby increasing flow speed in the channels. Thus, water flow and erosion are two important properties in heterogeneous topography formation.

Here in this section, we combine hydrodynamics, vegetation, and topography dynamics into one coupled model. Starting with introducing two dynamics used in the previous study, then we describe the shallow water equation as the surface water modeling and topography dynamics. The conceptual model of this study is depicted in Figure 2.1. Since we deal with high variance time-scales, three methods are discussed to tackle the issue. Further details regarding assumptions and limitations of the model are discussed in each section.

2.1.1 Vegetation Dynamics

In arid ecosystems, vegetation growth is limited to availability of water. Here, we treat water as two different dependent variables in this model, infiltrated water as soil water while run-off as surface water. Growth rate of vegetation is assumed to be limited to the amount of soil water available. It is defined as a multiplication of a half-saturation function of soil water with a constant k_1, water up-take rate, g_{max}, and conversion rate, c. Moreover, vegetation density is assumed to be loss due to vegetation life-span with mortality rate, d. Furthermore, vegetation in arid ecosystems can disperse spatially when neighboring areas with better resources are available. Here, the movement is modelled by a diffusion term with a coefficient, D_p. Thus, the phenomena above can be written as a mathematical expression which is given by,

$$\text{Biomass Dynamics} \rightarrow [\text{Growth}] - [\text{Death}] + [\text{Plants Dispersal}]$$

$$\frac{\partial p}{\partial t} = c g_{max} \frac{w}{w + k_1} p - dp + D_p \Delta p. \tag{2.1}$$

2.1.2 Soil Water Dynamics

Soil water, which come from infiltration of surface water, are absorbed by vegetation, evaporates, and are flowing through gaps inside the soil. Infiltrated water from the surface become the only water input in soil water dynamics. The infiltration rate is defined as a half-saturation function of vegetation density with a constant k_2. The maximum infiltration rate is α in vegetation patches while αw_0 in bare soil areas. Besides absorbed by vegetation, some amount of soil water will evaporate or seep out of system through drainage at linear rate r_w. Furthermore, we assume that the soil water can disperse through some gaps inside the soil due to capillary forces. The movement is describe with a diffusion term at a constant rate,

D_w. Thus, the soil water dynamics can be defined as a partial differential equation below,

$$\text{Soil Water} \rightarrow [\text{Infiltration}] - [\text{Water-uptake}] - [\text{Evaporation}] + [\text{Capillary Forces}]$$
$$\frac{\partial w}{\partial t} = \alpha h \frac{p + k_2 w_0}{p + k_2} - g_{max} \frac{w}{w + k_1} p - r_w w + D_w \Delta w. \tag{2.2}$$

2.1.3 Surface Water Dynamics

In arid ecosystems, rain (or rainstorms specifically) only happen in discrete events and in short-period of time. Here in the model, we assume the water input from rainfall is a continuous event and homogeneous. A specific amount of water is added throughout the spatial domain continuously. Therefore, it allows a thin-sheet water column flowing in the system during continuous period.

Surface water is modeled by using shallow water equations. The shallow water equations consist of two main equations, continuity and momentum equations. Water level depth characteristic in the shallow water equations, h, is assumed to be much smaller than the horizontal length of water column. Therefore, the surface water dynamics are considered to be more lateral than vertical directions.

Here in this section, we provide the explanations on how we implement shallow water equations into the arid ecosystems modeling. Beside that, we introduce one of wetting-drying algorithms to deal with dry areas in the shallow water equations.

Continuity Equation

Continuity equation explains the amount of water in the cells which depends on the amounts that are coming into and going out of the cells. In this model, we assume the water flow can be coming from x and y directions. Therefore the flux of water coming into and going out of the cell can be described as net fluxes which are the multiplication of water flow and column in x and y directions. Beside that, to complete the equation, we add one external source to model water input from rainfall and one external sink to describe water infiltration into soil. Then, we can have an adjusted continuity equation,

$$\text{Local Water Height Dynamic} + \text{Net Flux} \rightarrow [\text{Rainfall}] - [\text{Infiltration}]$$
$$\frac{\partial h}{\partial t} + \frac{\partial (hu)}{\partial x} + \frac{\partial (hv)}{\partial y} = R - \alpha h \frac{p + k_2 w_0}{p + k_2}. \tag{2.3}$$

On the left hand side, we have local height dynamics which depends on the net fluxes. The fluxes are determined by how fast water flow in x and y direction are coming into and out from the cell then multiplied by water columns. On the other side, rainfall is modeled as a constant input for all cells, R, and infiltration is modeled as a saturation function of vegetation density and availability of water. As the patches get denser, infiltration rate increases and then plateaus after passing the half saturation constant, k_2. In other cases, where is no vegetation present, infiltration rate is at the lowest value, αw_0.

Momentum Equations

The next component of shallow water equations is momentum equations. The equations describe how momentum in the water flow are changed and transferred between water column through the interactions with bed topography and gravity. The change in inertia is

modeled by local dynamics and convective accelerations. Here are the mathematical expression of the momentum equations,

$$\text{Local Inertia} + \text{Conv. Acc.} \rightarrow -[\text{Pressure}] - [\text{Friction Loss}] + [\text{Turbulent}]$$

$$\frac{\partial u}{\partial t} + u\frac{\partial u}{\partial x} + v\frac{\partial u}{\partial y} = -g\left(\frac{\partial(h+z+z_{ref})}{\partial x}\right) - S_{fx} + D_u\Delta u, \tag{2.4}$$

$$\frac{\partial v}{\partial t} + u\frac{\partial v}{\partial x} + v\frac{\partial v}{\partial y} = -g\left(\frac{\partial(h+z)}{\partial y}\right) - S_{fy} + D_v\Delta v, \tag{2.5}$$

with the bottom friction can be defined as a quadratic function of the velocities (Kämpf, 2009),

$$S_{fx} = \frac{g}{C^2h}u\sqrt{u^2+v^2}, \tag{2.6}$$
$$S_{fy} = \frac{g}{C^2h}v\sqrt{u^2+v^2},$$

and the coefficient C, Chézy coefficient, follows Baptist et al., 2007 in case of emergent vegetation,

$$C = \sqrt{\frac{1}{\frac{1}{C_b^2} + \frac{C_D p h}{2g}}},$$

where C_b and C_d represent bed roughness coefficient and bulk drag vegetation density.

In the model, pressure gradient consist of hydrostatic pressure and two slope gradient of topography. First gradient comes from the reference slope gradient which represented as z_{ref} while the other gradient, z, comes from an erodible bed topography. The last term on the right hand side represents turbulent "eddy" stress which is modelled by diffusion term with diffusion constants, D_u and D_v for x and y directions, respectively.

Wetting-Drying: Thin-film Algorithm

A deterministic mathematical model consider continuous processes that are happening in the dynamics instead of several discrete occurrences. Here we assume that an average annual rainfall is added into the all spatial grids in the system as a constant water input at every time step. However, when water flow gets accumulated in the channels, some areas are drier than the others. The shallow water equation cannot evaluate a cell with zero value of water depth due to the infinite friction loss (low water level h induces very high friction, see equation 2.6). Therefore, one needs to use a wetting-drying algorithm to shallow water equations continuing the computation process.

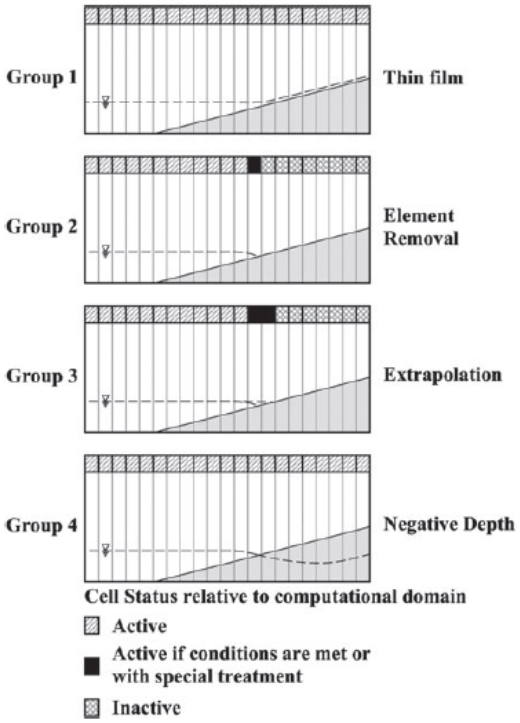

FIGURE 2.2: An illustration image to wetting-drying algorithms. The image is taken from Medeiros and Hagen, 2012. In this study, we implement the algorithm in group 1: thin-film algorithm.

Here we implement a thin-layer algorithm in mimicking wet and dry areas. We evaluate each cell using the shallow water equations and at the end of each iteration, the low water level cells (can be negative or zero value) are corrected by a thin layer of water, h_{min} while the rest remain the same. Therefore, dry areas would have a thin-layer of water as an input for shallow water equation while wet areas are not changed. The illustration of this method can be seen in Figure 2.2 on group 1. The benefit of this method is one does not need to remove any cells in the computation scheme and can use all cells on every iteration. Further explanations and other options regarding wetting-drying algorithms can be found in Medeiros and Hagen, 2012.

2.1.4 Bed Evolution Equation

Topography dynamics is modelled as two layer of beds. The first layer is called erodible dynamics bed while the second layer is non-erodible static bed. The non-erodible gives us a static slope gradient which also represents a hard rock layer on the earth crust. On the other hand, the erodible layers, which represent red sandy and silty sand, are changing over time due to soil erosion. Additional slopes will be given to the present slope as the erosion shaping up the topography. The illustration of these two layers of bed topography is depicted in Figure 2.3. Furthermore, we consider an external source in the topography dynamics as a constant tectonic up-lift to represent an external force keeping topography reference. Therefore, topography dynamics will be present as a non-uniform landscape in steady state condition instead of a flat eroded landscape.

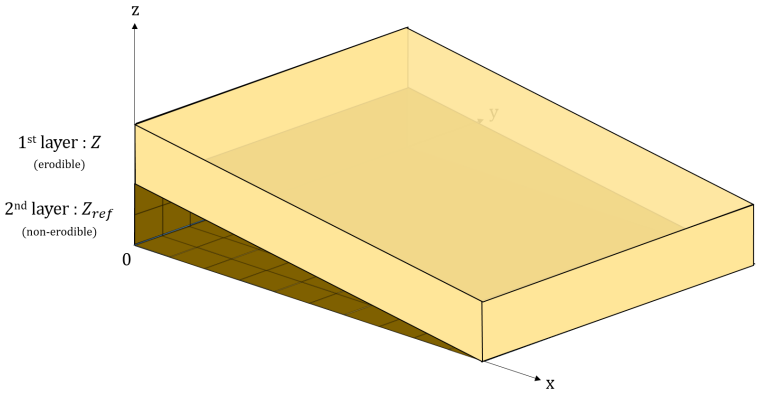

FIGURE 2.3: Landscape modeling using two layer of bed topography, one is flat and erodible, z, and the other is non-erodible that has a slope gradient, z_{ref}. These erodible and non-erodible layers represent red sandy - silty sand soil and hard rock layers, respectively.

The bed evolution modeling consists of three terms. Firstly, we model a constant tectonic up-lift as mentioned at the beginning of the section. The up-lift is computed by spatially averaging the erosion each iteration. Secondly, soil erosion modeling consists of maximum erosion rate, β_{max}, absolute speed of water flow, and effective water level. The erosion rates are vary as water flow are non-uniform. A concentrated flow enhances soil erosion due to an increased flow speed. Moreover, the height of water column improves the erosion rate since there is more capacity for sediments to be transported by the water flow. We model the enhancement by water level as a half-saturation function with a constant, κ. Lastly, we also add a soil dispersion as a diffusion movement at a constant rate, D_z to model small scale landslides. Here is the mathematical expression of the bed evolution equation,

$$\text{Local Bed Evolution} \rightarrow [\text{Tectonic Up-lift}] - [\text{Erosion}] + [\text{Soil Dispersion}]$$
$$\frac{\partial z}{\partial t} = U - \beta_{max}\sqrt{u^2+v^2}\frac{h_{eff}}{h_{eff}+\kappa}z + D_z\Delta z, \tag{2.7}$$

with $h_{eff} = h - h_{min}$ is the effective water level. Here we assume there is an external force from below that keeps bed reference in level through the addition of erodible soil. Therefore we can obtain a varied topography instead of a fully eroded landscape at the steady state condition. To do so, we calculate a spatially averaged value of the amount of soil eroded in the domain and apply it back to the domain as a constant input of uplift. In general, we can derive the tectonic uplift equation which is given by,

$$U = \frac{1}{L_x L_y}\int_0^{L_x}\int_0^{L_y} E(x,y)dxdy,$$

where L_x and L_y represent the length of observation in x and y directions, and,

$$E(x,y) = \beta_{max}\sqrt{u(x,y)^2+v(x,y)^2}\frac{h(x,y)}{h(x,y)+\kappa}z(x,y).$$

The equation of U is derived from computing a volume under a surface which is characterized by a function of two variables as derived in Varberg, Purcell, and Rigdon, 2007 and then divided by the area of the domain to obtain the average value.

2.1.5 Time-scale Differences

Coupling hydrodynamics, vegetation dynamics, and topography dynamics increases the complexity of the model. Each dynamics has its own time scale of evolution to see noticeable changes (see Figure 2.4). Hydrodynamics is changing at very fast time scale i.e. seconds whereas vegetation could show the growth or colonization progress in days or even months. Moreover, topography dynamics has even longer time scale to be established, i.e. years or decades. Using a straightforward computation, one could obtain a reliable solution which represents the accurate physical phenomenon. However, it would cost very expensive computations and take really long time since a small change in topography dynamics need a large number of hydrodynamics iterations. Therefore, we need to include an assumption to tackle this issue. Here in this section, we would like to discuss three options that can be chosen to handle the large difference in time scales.

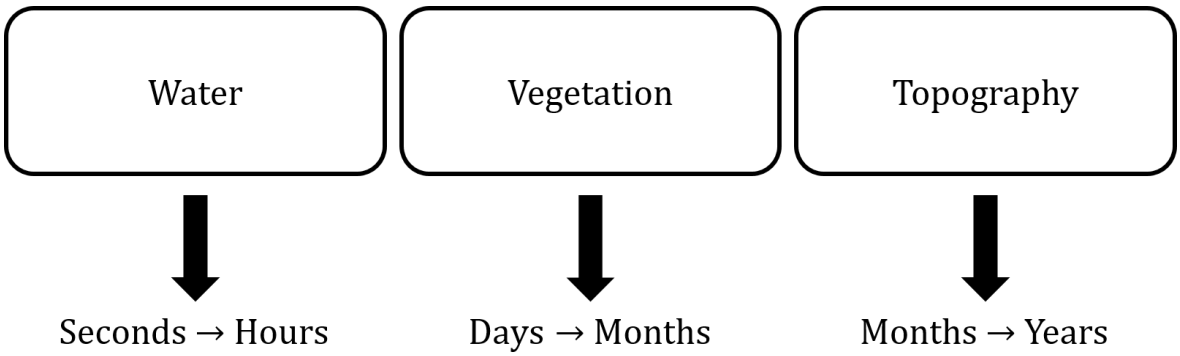

FIGURE 2.4: A scheme of time-scale differences between hydrodynamics, vegetation growth, and bed evolution in the proposed model.

Quasi-Steady State Approximation

One of the well-known methods to solve different time scale dynamics is quasi-steady state approximation or quasi-steady state assumption. This method was firstly introduced in Segel and Slemrod, 1989 and mainly used in the biochemistry field. In this method, it is assumed that if one or more dynamics in the system appear to be constant over time interval concerned, then we can approximate the dynamics equal to zero over time. Thus, the fast dynamics become independent of time.

Many scientists usually apply this method to reduce the complexity of the differential equations by removing one or more equations. One of the examples is in Weerman et al., 2010; they reduce the number of differential equations from three equations into two equations because one of the dynamics can be expressed algebraically independent of time using the method. Therefore, by using this method, we can simplify the system of partial differential equations and reduce the complexity.

Pseudo-transient Method

A numerical method called pseudo-transient method can also handle the time scale differences by utilizing multiple time scale computations. Instead of reduce the number of equations, firstly, we can simulate the fast dynamics until it reaches steady state and then use the result as an input for the slow dynamics. After the slow dynamics is updated, then the result becomes an input for the fast dynamics to reach a new steady state solution. The processes are going on until it reaches a prescribed time period concerned. The examples of the implementation of this method can be found in Simpson and Castelltort, 2006 and Saco,

Willgoose, and Hancock, 2007. This method has advantage that we could still use same equations without changing the meaning. However, the method will impose an expensive computation time due to multiple iteration stages. Thus, a justification between simple computation method and computation time is needed to obtain more realistic solutions or less waiting time.

Morphological Speed-up Factor

Another option to deal with different time scales is by speeding up the update process in the slow dynamics to keep up with the fast dynamics. This method is called morphological speed-up factor. In principle, the method favors the parameters in slow dynamics to be multiplied by a specific magnitude to allow the rate of change to be close enough to the fast dynamics (Ranasinghe et al., 2011). However, in some cases, this method might be not ideal because it may overestimate the impact, for example the fast dynamics has a crucial influence to the slow dynamics. Therefore, a balance between realistic results and computation time need to be considered in this case.

In this study, we use the morphological speed-up factor to produce simulation results. We increase the impact of hydrodynamics changes to vegetation and topography dynamics. Therefore, all three dynamics become in a same time scale period. Here are the explanation how we implement the speed-up factor,

$$\begin{aligned}
\frac{1}{\varphi_1}\frac{\partial w}{\partial t} &= \alpha h \frac{p + k_2 w_0}{p + k_2} - g_{max}\frac{w}{w + k_1}p - r_w w + D_w \Delta w, \\
\frac{1}{\varphi_1}\frac{\partial p}{\partial t} &= c g_{max}\frac{w}{w + k_1}p - dp + D_p \Delta p, \\
\frac{1}{\varphi_1}\left[\frac{\partial h}{\partial t} + \frac{\partial (hu)}{\partial x} + \frac{\partial (hv)}{\partial y}\right] &= R - \alpha h \frac{p + k_2 w_0}{p + k_2}, \\
\frac{1}{\varphi_2}\frac{\partial z}{\partial t} &= U - \beta_{max}\sqrt{u^2 + v^2}\frac{h - h_{min}}{(h - h_{min}) + \kappa} z + D_z \Delta z.
\end{aligned}$$

We do not apply the morphological factor into the momentum equations as it is already in seconds time scale. Then, we have the adjusted parameters as follow,

$$\begin{aligned}
\frac{\partial w}{\partial t} &= \varphi_1 \alpha h \frac{p + k_2 w_0}{p + k_2} - \varphi_1 g_{max}\frac{w}{w + k_1}p - \varphi_1 r_w w + \varphi_1 D_w \Delta w, \\
\frac{\partial p}{\partial t} &= c\varphi_1 g_{max}\frac{w}{w + k_1}p - \varphi_1 dp + \varphi_1 D_p \Delta p, \\
\frac{\partial h}{\partial t} + \frac{\partial (hu)}{\partial x} + \frac{\partial (hv)}{\partial y} &= \varphi_1 R - \varphi_1 \alpha h \frac{p + k_2 w_0}{p + k_2}, \\
\frac{\partial z}{\partial t} &= \varphi_2 U - \varphi_2 \beta_{max}\sqrt{u^2 + v^2}\frac{h - h_{min}}{(h - h_{min}) + \kappa} z + \varphi_2 D_z \Delta z.
\end{aligned}$$

Therefore, we have ten adjusted parameters to the morphological factor, i.e. $\varphi_1\alpha$, $\varphi_1 g_{max}$, $\varphi_1 r_w$, $\varphi_1 D_w$, $\varphi_1 d$, $\varphi_1 D_p$, $\varphi_1 R$, $\varphi_2 U$, $\varphi_2 \beta_{max}$, and $\varphi_2 D_z$. The values of φ_1 and φ_2 are estimated in this study. Further study is needed to discuss reliable values for morphological speed-up factors in comparison with observational studies.

2.1.6 Initial and Boundary Conditions

A well-posed mathematical problem needs to have a set of initial and boundary conditions to complete a system of partial differential equations. Initial and boundary conditions are

prescribed in each case. In this study, we deal with a system of partial differential equations in two dimension. Therefore, we need to assign a set of initial conditions for each variable and boundary conditions for each boundary. Thus, our system of partial differential equations has a unique solution.

Initial Conditions

Initial condition is a prescribed condition of all variables at time is equals zero for all spatial domain. It also means that the starting conditions of all physical features that are going to evolve over time in the system dynamics. The problem is we usually do not know how the initial condition was. Therefore, we draw an assumption that the initial condition of the system comes from homogeneous steady state solutions which derived in A. Thus, we can obtain a system of partial differential equations that has a unique solution.

Boundary Conditions

Besides initial conditions, to solve a system of partial differential equations mathematically, we need to impose boundary conditions. Many options can be made to prescribe the boundary conditions. Here in this study, we explain three boundary conditions that are relevant to the current modeling concept.

Periodic Boundary
Periodic boundary is widely used for solving a system of partial differential equations which the solution is known analytically. This type of boundary allows matters, which go out of the system, come back into the system from the other side of boundary (Kämpf, 2009). The boundary is useful to impose infinite domain to our system. It means that the boundary of our computation is less restrictive. Therefore, this type of boundary is appropriate for simulations that are not limited to the condition of boundary.

Closed Boundary
A closed boundary is a boundary condition that does not allow matters to go out of the system. It is usually used to represent coastline or experimental wall setup. This boundary is classified into two types, no-slip and full-slip boundaries (Kämpf, 2009). No-slip boundary means flow or matters, that come toward the boundary, will be diminished due to zero flow condition at the boundary. In other words, no matter or flow is at the boundary. On the other hand, full-slip boundary allows water flow to be present but there is no exchange of flow at the boundary. Therefore, the normal derivative with respect to the direction of the flow is equals to zero.

Open Boundary
An open boundary is a counter condition of the closed boundary, instead of keeping matters or flow inside the system, it allows matters or flow go out of the system. Using this type of boundary, it is also possible to fix a source input at the boundary, for example tide waves as in the shore. Therefore, the idea of this type of boundary is to allow matters originating from the system leave the domain without influencing the interior solution. In this study, we focus on the open boundary that allows matters or flow go out of the system to simulate drainage channels.

2.2 Finite Difference Method

Most of cases in mathematical modeling of ecology incorporate non-linear interactions between compartments or variables. Finding analytic solutions of a system of partial differential equations is difficult due to the complexity of non-linear equations. Therefore, one usually implements a numerical method to approximate the solutions. However, the numerical solutions are not as accurate as the exact solutions because of an approximation of the smooth curve by several numbers of grids. The accuracy of numerical methods depend on how many terms are considered in the approximation. The more terms are ignored, the less precise the method is. In this section, we are going to explain a numerical method for approximating the solution of a system of partial differential equations which is called a finite difference method.

Finite difference method is a numerical method for solving differential equations by approximating the solution using difference equations LeVeque, 2007. The method proceeds by replacing the differential equations by finite difference equations then computes the solution using defined grids. The difference equations are derived from the Taylor series. Consider a Taylor series,

$$f(x+h) = f(x) + \frac{f'(x)}{1!}h + \frac{f''(x)}{2!}h^2 + \ldots, \tag{2.8}$$

with x is the independent variable and h is a step size. To approximate the first derivative, $f'(x)$, we can neglect the higher order terms and rearrange the equation. Then we can have,

$$f'(x) \approx \frac{f(x+h) - f(x)}{h}.$$

This approximation of the first derivative is called forward finite difference. The method approximates the derivative from one-sided since the derivative f' is estimated at a point x from the right side of h. There is another option of one-sided approximation which is given by,

$$f'(x) \approx \frac{f(x) - f(x-h)}{h}.$$

This approximation is called backward difference method. The illustration of both approximations can be seen in Figure 2.5. The slope gradient (red line) can be approximated by two options, the forward finite difference (yellow line) or the backward finite difference (purple line). In this case, as the slope gradient at x is positive, then forward difference estimate the derivative better than backward difference. However, in other cases, when the slope gradient x is negative, the backward difference performs better than a forward difference. Therefore, it is important to take the possible exact gradient into a consideration when using a numerical method.

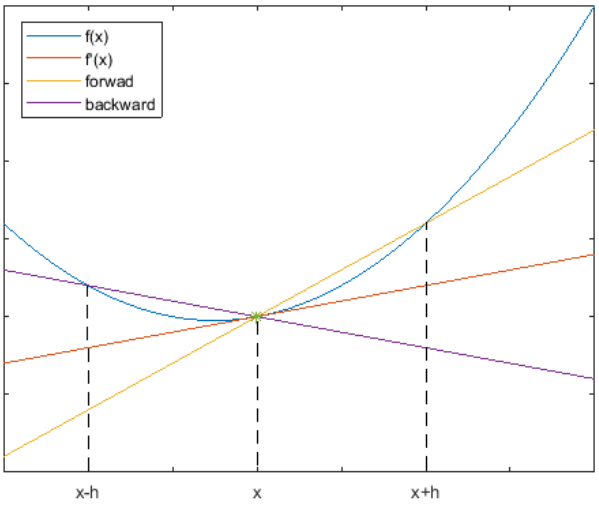

FIGURE 2.5: An illustration to finite difference methods. Forward-Backward difference are presented here.

In numerical methods, numerical accuracy and numerical stability are important measures to ensure that the solutions came from a convergence approximation. Both one-sided approximations explained above give a first order accurate of estimation. It means that the errors compared to approximated results are related in the first order of magnitude h. Therefore, when we reduce the grid size h to h^2, then the errors will be linearly reduced which is equal to a constant multiplied by h. Besides that, the numerical stability analysis is also an important feature to avoid numerical artifacts or numerical instability. As we approximate the solution in a finite number of grids, the numerical method should not amplify the error between the approximation and the exact solutions to obtain a stable solution. Therefore, it is necessary to take into account the numerical stability in the study.

In this section, we explain how we implement a finite difference method to approximate the spatial and temporal grids. For the spatial grids, we perform a centered finite differences method to avoid the effects of the precondition of the slope gradient. We also introduce the two approximation method for the time integration, i.e., explicit-implicit method and the Runge-Kutta method. Furthermore, we consider two stability criteria for numerical approximations, i.e., Courant-Friedrich-Lewy condition and Mesh Péclet number, to ensure the solution is numerically stable.

2.2.1 Spatial Grid Approximation

This study works with two-dimensional space of x and y and a temporal grid. To obtain the solutions of our system, we discretize our spatial into several numbers of uniform grids. The size of grids in x and y axes is also the same. To obtain higher accuracy results, we impose centered finite difference method into our spatial grids. This method has a second order of accuracy meaning that it is more precise than the two methods discussed before. Further, we discuss mesh Péclet number as a numerical stability criterion for spatial approximation.

Centered Finite Differences

Centered finite differences method approximates the slope at the center based on the average value of two-sided approximations. In short, mathematically, we consider its neighbor

values instead of itself,

$$f'(x) \approx \frac{f(x+h) - f(x-h)}{2h} = \frac{1}{2}\left(\frac{f(x+h) - f(x)}{h} + \frac{f(x) - f(x-h)}{h}\right).$$

The illustration of this method can be found in Figure 2.6. The advantages of this method are simple in the implementation and more accurate than the one-sided approximation. This approximation has a second order of errors h^2 meaning that as we impose a higher number of grids, the error will be reduced quadratically.

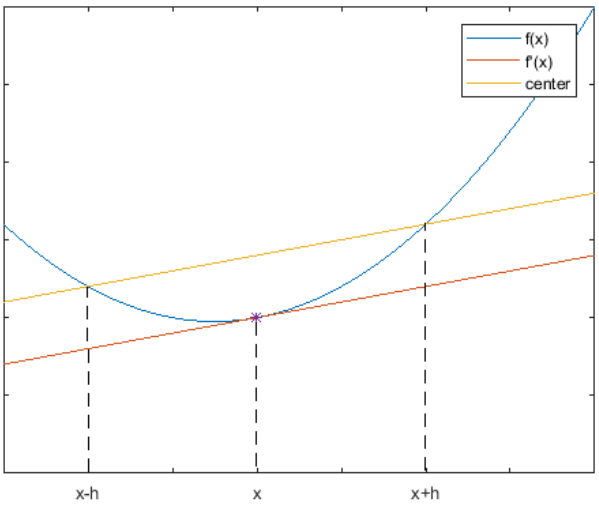

FIGURE 2.6: An illustration to center finite difference methods. Centered finite difference (yellow line) approximates the slope of the function $f(x)$ by averaging two-sided approximations.

In our system, we have two types of spatial derivative, first (advection) and second (diffusion) order derivatives. Lets consider $\mathbf{u}$ is a discrete approximation of function f. Then using this method, we can approximate the derivatives as follows,

$$\left.\frac{\partial \mathbf{u}}{\partial x}\right|_{x_i=i} \approx \frac{\mathbf{u}_{i+1} - \mathbf{u}_{i-1}}{2\Delta x},$$
$$\left.\frac{\partial^2 \mathbf{u}}{\partial x^2}\right|_{x_i=i} \approx \frac{\mathbf{u}_{i+1} - 2\mathbf{u}_i + \mathbf{u}_{i-1}}{\Delta x^2},$$

with Δx is a spatial grid size. However, in some cases, this method could produce unstable oscillatory solutions due to method inability to dampen the errors. The sign of oscillation emergence is described in mesh Péclet number.

Mesh Péclet number

The oscillatory solution may emerge in the system of partial differential equations which has an advection-diffusion equation when we use centered finite difference method. To avoid the oscillatory behavior, we need to keep Péclet number as low as possible. The number is a dimensionless value which compute the ratio between the advection and diffusion rate.

From the article by Veldman, 2001, the Péclet number is defined as,

$$Pe = \frac{u}{D_u}\Delta x,$$

or in general, when we have a two dimensional system, we can rewrite the equation above as follows,

$$Pe = \frac{\sqrt{u^2 + v^2}}{max(D_u, D_v)}\Delta x,$$

with Δx represents the spatial grid size, u, v are water flow velocity in x and y directions, and D_u, D_v are diffusion constants. The numerator represents the absolute velocity in a grid while the denominator represents the maximum value between diffusion constants in x and y directions. Large Péclet number corresponds to a higher influence of advection instead of diffusion transport. Therefore, in advection-dominated flow, we could consider diffusion as zero. However, in the cases where diffusion transport is essential, we need to consider taking finer grids as small as possible. The balance between computation time and realistic parameters are essential in mathematical modeling to ensure that our model generates a reliable solution.

2.2.2 Time Integration Method

The approximation for time derivative is discussed here. The simplest method in approximating time derivative is forward Euler method another name of forward difference method. The method is included in a category of explicit computation methods. The explicit computation means that we can calculate the next time step directly based on the solution at present. Similarly to backward difference, in time integration method, we also have a method so-called backward Euler. In this method, instead of computing the next time step directly, we need to compute the backward operator inversely to calculate the next time step. Because of this inverse computation, this method is also called an implicit method. Explicit method is way easier to implement compared to implicit method since inverse computation is quite heavy and complicated. However, in most cases, the explicit method is more numerically unstable than the implicit method. Other option between the two explicit-implicit scheme, there is a method called semi-implicit. In this method, we still have the straightforward computation to obtain the solution, but we could include several newly computed results into the explicit computation. Therefore, the advantage of the implicit method can be utilized while using the explicit method.

Finally, we would like to explain one another time integration method, which is called the Runge-Kutta 4th order. This method is still a family of the explicit methods but using several mid-steps before computing the one full time step solution. Therefore, the Runge-Kutta method has more predictive power than the other options here.

Explicit Scheme

Lets consider a system of partial differential equations as follows,

$$\frac{\partial \mathbf{u}}{\partial t} = f(t, \mathbf{u}),$$

where $\mathbf{u}$ is a vector of dependent variables and f is a spatial interaction function, for instance, a reaction-diffusion function. In the explicit scheme, we can compute the dependent

variables for the next time step directly from known variables and parameters at the moment. A well-known explicit method is the forward Euler method which can be expressed as follows,

$$\mathbf{u}^{n+1} = \mathbf{u}^n + \Delta t f(t^n, \mathbf{u}^n),$$

where Δt is a temporal step size, n is an index of time and $f(t, \mathbf{u})$ is a discretization of spatial interaction function. The method is easy to implement in any system of differential equations and quite straightforward. However, the option to chose the temporal step size is limited to a Courant-Friedrich-Lewy condition in which the size of time step should be sufficiently small to avoid non-physical meaning attributed to the next computation.

Courant-Friedrich-Lewy Condition
Courant-Friedrich-Lewy criterion is a necessary condition for solving partial differential equations numerically to obtain a stable solution. The criterion is based on stability analysis of numerical methods. The condition states that the numerical methods must be used in such a way that all the computation come from physically meaningful grids. In other words, the grid size of computation (both spatial and temporal) must be sufficient enough to incorporate the source grids that have correct physical meaning (Weisstein, 2018). For one dimensional case, CFL condition, λ, of shallow water equations is defined by (Kämpf, 2009),

$$\lambda = \frac{\Delta t}{\Delta x}\sqrt{g h_{max}} \leq 1,$$

where $\Delta t, \Delta x$ are temporal and spatial grid sizes, g is gravity acceleration and h_{max} is the maximum water depth encountered in the system. If we expand the condition to the two dimensional case, we can have,

$$\lambda = 2\Delta t\sqrt{g h_{max}}\sqrt{\frac{1}{\Delta x} + \frac{1}{\Delta y}} \leq 1.$$

Because of its attribute as a necessary condition, if this condition is violated then the method will be not convergence to the solutions while if this condition is satisfied, the method might be convergence. However, the actual stability analysis must be conducted to prove the convergence.

Semi-implicit Method
Other option to relax the necessary condition is a semi-implicit method. This method utilizes the newly computed variables from the next time step into the following variables. It means that there are several variables which are computed in the same time step whereas the other computed in mixed time step. The semi-implicit method can be described as follows,

$$\mathbf{u}^{n+1} = \mathbf{u}^n + \Delta t f(t^n, \mathbf{u_1}^n, \mathbf{u_2}^{n+1}),$$

where $\mathbf{u}_1$ and $\mathbf{u}_2$ are chosen at different time steps. Since this method is still categorized as a family of explicit methods, parameter of choices needs to follow the Courant-Friedrich-Lewy condition.

Runge-Kutta Method
Runge-Kutta method is one of an explicit numerical method which includes multistage approximation in time integration. Instead of calculating the next time step in one go, this

method computes the average of multiple time integration between one step. There are numerous options of Runge-Kutta methods; we consider the Runge-Kutta 4th order method in this study. The fourth order means that we average four multiple steps between one-time step and it also has 4th order accuracy. Here are the mathematical expression of this method,

$$\mathbf{u}^{n+1} = \mathbf{u}^n + \frac{\Delta t}{6}(k_1 + 2k_2 + 2k_3 + k_4),$$

where the k_1, k_2, k_3 and k_4 are defined as,

$$\begin{aligned} k_1 &= f(t^n, \mathbf{u}^n), \\ k_2 &= f(t^n + \frac{\Delta t}{2}, \mathbf{u}^n + \frac{k_1}{2}), \\ k_3 &= f(t^n + \frac{\Delta t}{2}, \mathbf{u}^n + \frac{k_2}{2}), \\ k_4 &= f(t^n + \Delta t, \mathbf{u}^n + k_3). \end{aligned}$$

The first step, k_1 means that we compute the slope using forward Euler while k_2 and k_3 means that we calculate the slope in the half-way computation using k_1 and k_2 as an input, respectively. The last step is the corrector step which means we compute the full step slope using k_3 as an input. Thus, we can compute each one step of iteration entirely using average multiple time steps.

Using the Runge-Kutta method, we can acquire more accurate computation compared to forward Euler and could relax the Courant-Friedrich-Lewy condition. This method also helps the calculation to avoid divergent numerical solutions better than the forward Euler and semi-implicit method. However, the computation time of this method is higher than the forward Euler due to additional middle steps. To compete for the speed of the forward Euler computation, we could also increase the time step in this method. Therefore, we could obtain a better computation time with reasonable results. Thus, the balance between computation time and accuracy become an important feature that needs to be into consideration.

2.3 Model Analysis

In this section, we explain how we analyze numerical simulation results of the proposed model. Firstly, we describe continuation method which is used to simulate the impact of environmental changes on the arid ecosystems. Secondly, we present spectral analysis method to analyze regularity of spatial patterns emerged from the system. After that, we provide default initial setups of the model which consist of initial-boundary conditions, parameters, and discretizations. Lastly, further explanations on how we set up scenarios to mimic environmental changes, i.e., decreasing/increasing rainfall, are discussed in this section.

2.3.1 Continuation Method

The idea of the continuation method is to compute steady-state solutions if one or more parameters are varied (Meijer, Dercole, and Oldeman, 2009). Numerical continuation method is usually used to conduct the stability analysis of a non-linear system of equations. Stability of steady states has become an important indicator in ecological studies since it can predict the condition of ecosystems in a long period of time. If the steady-state solutions are unstable, it means that by using a small perturbation, the solutions will shift to new stable steady-state solutions or lie in a continuous cycle (on limit cycle trajectories). On the other case, if the steady-state solutions are stable, then it has a certain level of resilience towards

perturbations that keeps it stays in undisturbed conditions. Therefore, it is essential to know the stability of the steady state solutions for an ecosystem modeling as a tool to simulate a long period of time evolution.

In the proposed model, we have a system of six non-linear partial differential equations and more than 20 parameters. Numerical computation is very limited to the complexity of the system. Therefore, we implement the simplest continuation method available in the current project. Firstly, we compute the approximated solution by using the finite difference method. The simulations run until it reaches a steady-state condition. However, instead of calculating the approximated the steady-state solutions by using iterative methods (for example, Newton method), we run the simulations until the change in spatially averaged vegetation density is small enough (in a degree of 10^{-2}) to ensure that the system is in a steady-state condition. Secondly, after we obtain the steady-state solutions, small magnitude perturbations are imposed and distributed spatially to the vegetation density in 0.05% of random patches. Then, we rerun the numerical method by using the new parameter value and the previous result as a new initial condition. The procedures continue until we obtain the prescribed the end value of the parameters.

2.3.2 Spectral Analysis

Regular spatial patterns usually can show a particular periodicity at a certain magnitude. This periodicity is usually subjected to a specific wavelength. In an arid ecosystem, the pattern is generated by the interspersed patches between vegetation and bare soil. Wavelength determines a distance between two different vegetation patches or bare soil areas. In most cases, patterns have a specific directional component with a certain magnitude to see repeated arrangements. The wavelength analysis should be conducted in the same direction as the directional component to obtain a proper calculation. However, in other cases, the patterns can have several directional components that will increase the complexity of pattern analysis. A circular pattern, for instance, has almost one full circle directional components in order to find a repeating pattern. Therefore, to analyze the regularity of spatial pattern, we need a tool which can account for the wavelength and the orientation of the pattern.

Here in this section, we introduce a method to investigate the wavelength and the orientation of a regular spatial pattern which is called spectral analysis. This method explains a pattern wavelength and orientation by using three different statistics; periodogram, radial spectrum, and angular spectrum. A periodogram is a transformed dataset by cosine waves at different frequencies or wavenumbers. This transformation allows us to create the proportion of the image variance thereby giving us the information regarding periodicity in the data. On the other hand, radial spectrum method is a way to collect information regarding the scale of the pattern by binning the elements of periodogram for which have a same frequency. Lastly, the orientation of spatial patterns is determined by the radial spectrum in which the values of periodogram are binned based on angular segments. The full explanation of this method can be found in Renshaw and Ford, 1984, then the implementation can be found in Couteron and Lejeune, 2001, and Koppel et al., 2005.

Periodogram

Before calculating the periodogram, the data set, Y_{mn} with m and n denoting size, are scaled by mean-corrected value. This method are shifting the average value of the data set to zero. Denote this mean-corrected data set by X_{st}, where $s = 1, ..., m$ and $t = 1, ..., n$. Periodogram,

I_{pq} can be calculated by using equations below,

$$I_{pq} = mn(a_{pq}^2 + b_{pq}^2),$$

where

$$a_{pq} = \frac{1}{mn} \sum_{s=1}^{m} \sum_{t=1}^{n} X_{st} \cos \left[2\pi \left(\frac{ps}{m} + \frac{qt}{m} \right) \right],$$

and

$$b_{pq} = \frac{1}{mn} \sum_{s=1}^{m} \sum_{t=1}^{n} X_{st} \sin \left[2\pi \left(\frac{ps}{m} + \frac{qt}{m} \right) \right],$$

for $p = 0, ..., m-1$ and $q = 0, ..., n-1$. Image variances, which correlates to periodicity, in the data set would get amplified by applying this transformation. Therefore, the periodogram allows us to analyze the approximation of wavenumber and orientation of the pattern.

Radial and Angular Spectrum

Radial and angular spectrum analyses are conducted by counting and binning the values of periodogram, I_{pq}, which are related to each wavenumber and each orientation. First, we define the interval of the bin in which the values will be collected, i.e., ten bins are equals to 10 different intervals of 180 degrees, then we can have $0 \leq \theta \leq 10^o$, $11^o \leq \theta \leq 20^o$,... On the other hand, for the radial spectrum, define $r = \sqrt{(p^2 + q^2)}$ as one wavenumber group then do the same procedure for each p and q. The collected data are clustered into each wavenumber and also its orientation by using these two bins. Then, both spectrums are rescaled by using dataset variance. Thus, the distribution of radial and angular spectrum can be presented in each wavenumber and each angle, respectively.

2.3.3 Initial Setup

The default setup of the simulations is discussed here. First, we describe initial and boundary conditions which are used in the numerical simulations. After that, we modify the parameters based on the article Rietkerk et al., 2002 by using the morphological speed-up factor. At the end of the section, we describe how we implement the finite difference method to discretize the differentials.

Initial and Boundary Conditions

In this study, initial conditions are obtained from the homogeneous steady state solutions of our system. The derivation of the solutions can be found in A. Therefore we can have the initial condition for each variable as follows,

$$\begin{aligned} \bar{w} &= \frac{R}{r_w}, \\ \bar{h} &= \frac{R}{\alpha w_0}, \\ \bar{u} &= 0, \\ \bar{v} &= 0. \end{aligned}$$

To allow self-organized spatial patterns, we introduce a high density of vegetation, $\bar{p}$, which inhabits 5% of all cells. For the initial bed topography, $\bar{z}$, we impose two layers of bed topography, the top layer is a flat erodible soil with 2.5 meter thickness and spatial random perturbations between 0 and 0.1, and the bottom layer is a non-erodible layer that has a slope gradient, 0.25%, along x axis. The direction of the slope is from the left (up-slope) to the right (down-slope) boundaries. The illustration of the initial conditions of vegetation and bed topography can be found in Figure 2.7.

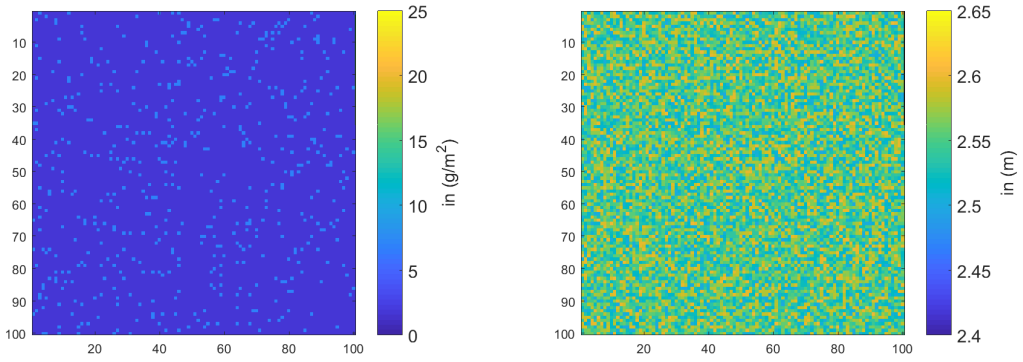

FIGURE 2.7: Initial conditions for vegetation density, $\bar{p}$, and erodible bed topography $\bar{z}$. The trivial homogeneous steady state of vegetation density is perturb by 5% of cells with a high vegetation density while a random spatial distribution of noise is added to erodible bed topography.

The default setup of the boundary condition for all four boundaries is the periodic boundary condition. Matters and flow can go out of and return to the system through the two boundaries facing each other. We implement this type of boundary to let the area of interest which is not restricted to the boundary condition.

Parameters

Parameters are obtained from the article Rietkerk et al., 2002 with several adjustments. We transform unit parameter used in the article, mm/day, into universal unit parameter, m/s. Therefore, we have parameter values in a same time scale. Moreover, using this method, we can continue our computations with the current equations. As discussed in the section 2.1.5, we impose a speed-up factor φ_1 which is equals to 10,000 times. In this study, the speed-up factor is estimated based on our period of interest. Further study is needed to justify the estimated value for speed-up factor. The summary of parameter values are presented in Figure 2.1.

TABLE 2.1: Value of all parameters used in the numerical simulations before multiplied by a speed-up factor (except topographic parameters).

Parameter	Description (Unit)	Value
φ_1	Speed-up factor for vegetation (-) density	10^4
φ_2	Speed-up factor for topography (-) dynamics	-
α	Maximum infiltration rate (s^{-1})	2.32×10^{-6}
k_2	Half-saturation constant for infiltration rate (g/m^2)	5
w_0	Maximum infiltration rate of bare soil (-)	0.06
g_{max}	Maximum water uptake rate by vegetation ($m^3/(gs)$)	5.79×10^{-10}
k_1	Half-saturation constant for water up-take (m)	0.005
r_w	Drainage and evaporation rate ($1/s$)	2.32×10^{-6}
D_w	Diffusion coefficient for soil water dispersal (m^2/s)	1.16×10^{-6}
c	Conversion rate (g/m^3)	10^4
d	Senescence rate of vegetation ($1/s$)	2.89×10^{-6}
D_p	Diffusion coefficient for vegetation (m^2/s)	1.16×10^{-5}
R	Range of average constant rainfall (mm/s)	$(0 - 1.16) \times 10^{-8}$
$\frac{dz_{ref}}{dx}$	Slope gradient of reference (unerodible) bed (-)	0.25%
C_b	Chézy friction coefficient for bottom ($\sqrt{m}/s$)	20
C_v	Chézyzy friction coefficient for vegetation (-)	0.2
D_u, D_v	Diffusion constant for turbulent "eddy" stress (m^2/s)	0.006
z_{base}	Amount of erodible bed layer (m)	2.5
$\varphi_2 U$	Tectonic up-lift (m/s)	-
$\varphi_2 \beta_{max}$	Maximum erosion rate (s/m^2)	4.75×10^{-4}
κ	Half-saturation constant for water flow capacity (m)	0.05
φD_z	Diffusion constant for soil dispersion (m^2/s)	0.0425

Discretizations

We implement a technique called method of lines to solve the system of partial differential equations. This method allows discretization of all dimension except one intended derivative (LeVeque, 2007). We discretize two spatial dimensions in x and y directions by using centered finite difference. Therefore, we can have a system of ordinary differential equations which only depends on the variable t. For temporal derivative, we apply an explicit time integration, Runge-Kutta 4th order, as a final step. We set up 100 by 100 of spatial grids which represent 1 km by 1 km area of interests ($dx = dy = 10$ meters) while for the temporal domain, we simulate each case for about 20,000 seconds or more than five hours which represent about six years of real observation with time step $dt = 0.1$ second. Thus, we can

have a semi-discrete system which is defined by,

$$
\begin{aligned}
\left.\frac{\partial p}{\partial t}\right|_{(x_i,y_j)=(i,j)} &\approx cg_{max}\frac{w_{i,j}}{w_{i,j}+k_1}p_{i,j} - dp_{i,j} \\
&\quad + D_p\left[\frac{p_{i+1,j}-2p_{i,j}+p_{i-1,j}}{\Delta x^2} + \frac{p_{i,j+1}-2p_{i,j}+p_{i,j-1}}{\Delta y^2}\right], \\
\left.\frac{\partial w}{\partial t}\right|_{(x_i,y_j)=(i,j)} &\approx \alpha h_{i,j}\frac{p_{i,j}+k_2w_0}{p_{i,j}+k_2} - g_{max}\frac{w_{i,j}}{w_{i,j}+k_1}p_{i,j} - r_w w_{i,j} \\
&\quad + D_w\left[\frac{w_{i+1,j}-2w_{i,j}+w_{i-1,j}}{\Delta x^2} + \frac{w_{i,j+1}-2w_{i,j}+w_{i,j-1}}{\Delta y^2}\right], \\
\left.\frac{\partial h}{\partial t}\right|_{(x_i,y_j)=(i,j)} &\approx R - \alpha h_{i,j}\frac{p_{i,j}+k_2w_0}{p_{i,j}+k_2} \\
&\quad - \frac{h_{i+1,j}u_{i+1,j}-h_{i-1,j}u_{i-1,j}}{2\Delta x} - \frac{h_{i,j+1}v_{i,j+1}-h_{i,j-1}v_{i,j-1}}{2\Delta y}, \\
\left.\frac{\partial u}{\partial t}\right|_{(x_i,y_j)=(i,j)} &= -g\frac{\eta^x_{i+1,j}-\eta^x_{i-1,j}}{2\Delta x} - Sc_{fx} \\
&\quad - u_{i,j}\frac{u_{i+1,j}-u_{i-1,j}}{\Delta x} - v_{i,j}\frac{u_{i,j+1}-u_{i,j-1}}{\Delta y} \\
&\quad + D_u\left[\frac{u_{i+1,j}-2u_{i,j}+u_{i-1,j}}{\Delta x^2} + \frac{u_{i,j+1}-2u_{i,j}+u_{i,j-1}}{\Delta y^2}\right], \\
\left.\frac{\partial v}{\partial t}\right|_{(x_i,y_j)=(i,j)} &= -g\frac{\eta^y_{i,j+1}-\eta^y_{i,j-1}}{2\Delta y} - Sc_{fy} \\
&\quad - u_{i,j}\frac{v_{i+1,j}-v_{i-1,j}}{\Delta x} - v_{i,j}\frac{v_{i,j+1}-v_{i,j-1}}{\Delta y} \\
&\quad + D_v\left[\frac{v_{i+1,j}-2v_{i,j}+v_{i-1,j}}{\Delta x^2} + \frac{v_{i,j+1}-2v_{i,j}+v_{i,j-1}}{\Delta y^2}\right], \\
\left.\frac{\partial z}{\partial t}\right|_{(x_i,y_j)=(i,j)} &= Uc - \beta_{max}\sqrt{u^2_{i,j}+v^2_{i,j}}\frac{h_{i,j}}{h_{i,j}+\kappa}z_{i,j} \\
&\quad + D_z\left[\frac{z_{i+1,j}-2z_{i,j}+z_{i-1,j}}{\Delta x^2} + \frac{z_{i,j+1}-2z_{i,j}+z_{i,j-1}}{\Delta y^2}\right],
\end{aligned}
$$

with $\eta^x = h + z + z_{ref}$ for x direction and $\eta^y = h + z$ for y direction. Moreover, the discretized friction function and tectonic up-lift are defined as,

$$
\begin{aligned}
Sc_{fx} &= \frac{g}{C^2 h_{i,j}}u_{i,j}\sqrt{u^2_{i,j}+v^2_{i,j}}, \\
Sc_{fy} &= \frac{g}{C^2 h_{i,j}}v_{i,j}\sqrt{u^2_{i,j}+v^2_{i,j}}, \\
Uc &= \frac{1}{N_x M_y}\sum_{i=1}^{N_x}\sum_{j=1}^{M_y}\beta_{max}\sqrt{u^2_{i,j}+v^2_{i,j}}\frac{h_{i,j}}{h_{i,j}+\kappa}z_{i,j},
\end{aligned}
$$

with N_x and M_y are the number of grids in x and y directions. If we assume all the equations on the right hand side are a discrete operator $F = L + M$ in which L is a linear operator and

M is a non-linear operator, then we can implement the time integration method as follow,

$$\mathbf{U}^{n+1} = \mathbf{U}^n + \frac{\Delta t}{6}(K_1 + 2K_2 + 2K_3 + K_4) \qquad \text{with} \qquad \mathbf{U} = \begin{bmatrix} p_{i,j} \\ w_{i,j} \\ h_{i,j} \\ u_{i,j} \\ v_{i,j} \\ z_{i,j} \end{bmatrix},$$

where the K_1, K_2, K_3 and K_4 are defined as,

$$\begin{aligned} K_1 &= F(\mathbf{U}^n), \\ K_2 &= F(\mathbf{U}^n + \frac{K_1}{2}), \\ K_3 &= F(\mathbf{U}^n + \frac{K_2}{2}), \\ K_4 &= F(\mathbf{U}^n + K_3). \end{aligned}$$

2.3.4 Scenarios

In this study, we are interested in looking at the resilience of the ecosystem towards environmental changes and the emergence of "feather" pattern. To do so, we simulate three scenarios, i.e., decreasing/increasing rainfall and open boundary condition (to let water leave out of the system). Here in this section, we present an explanation on how we implement these three scenarios. Any other configurations, which are not prescribed, will refer to the initial setup as a default.

Scenario 1: Land Degradation

Water as a primary resource in arid ecosystems provide all nutrients that are beneficial for vegetation. A scarcity of rain occurrences in arid areas leads to a potential threat for being degraded. It is predicted that rainfall is going to be less common in dry areas (Hendrix and Salehyan, 2012). This environmental change could influence vegetation pattern in arid ecosystems. In this thesis, we study how this environmental change influences the resilience of arid ecosystems towards environmental changes.

Ecosystem resilience can be tested by simulating environmental changes in the system. The term "resilience" means a capacity of ecosystems to respond to a perturbation or disturbance. To study the resilience of the ecosystem, we can use the continuation method to test the stability of steady state solutions toward a small perturbation whether it is still stable or shifted to a new equilibrium. Because of rainfall pattern in dry areas is predicted to be less frequent, we use an average annual rainfall to be the bifurcation parameter. Thus, we can analyze the process of land degradation by looking at the ecosystem resilience.

The simulation setup is discussed here. Starting with a gently sloped landscape, we simulate the emergence of vegetation bands in high rainfall (1 mm/day). Then, we apply the continuation method by reducing the amount of rainfall and introducing spatial random perturbations to vegetation density. On each iteration, we run the simulation until obtaining a new stable equilibrium. Rainfall parameter is reduced by 0.05 mm/day each simulation step until it reaches zero rainfall, 0 mm/day (21 rainfall parameters ranging from 0 to 1 mm/day). Thus, the simulation setup allows us to investigate the influence of external disturbance toward vegetation and topography in arid ecosystems.

Scenario 2: Vegetation Colonization

In this scenario, we are interested in the other possibility of increased rainfall to the vegetation pattern in arid ecosystems. It has been suggested by many (Siteur et al., 2014, Sherratt, 2015) that vegetation patterns can be developed from bare soil with a lower wavelength before turning into uniform vegetation state at steady state condition as rainfall is getting higher. Furthermore, the other previous studies (Scheffer et al., 2001, Rietkerk et al., 2004) suggested that a possible case of hysteresis in which the ecosystem mechanism fails to recover vegetation patches due to no concentration of water feedback. However, they have not included the effect of topography on the vegetation patterns in their results. In the presence of topography dynamics, it is possible that topographic variance is developing during a long dry period which thereby providing water catchment areas as depressions and channels. Furthermore, as water distribution is not uniform, local vegetation growth are different between low and high topography which then turning the "stripes" bands into "arcs".

Here, we would like to investigate the impact of feedbacks between vegetation and topography on the origin of vegetation "arced" bands in arid ecosystems. The simulation setup is the same with the previous scenario except we start with low rainfall.

Scenario 3: Open Boundary Condition

In scenarios 1 and 2, we impose periodic boundary to simulate the infinite domain. It means there is no way matters can escape from the system instead of through local removal (for example natural death or evaporation). However, drainage "feather" patterns come from a limited or finite domain because up-slope topography is found to be higher than the down-slope. In this scenario, we would like to impose an open boundary condition for one of the boundaries to let matters go out of the system. Meanwhile, on the other three boundaries, we implement a wall boundary condition. This type of boundary is implemented by using two mathematical boundary conditions. First, for the flow through the boundary, we implement Dirichlet boundary condition, $(u, v) = (0, 0)$ while the tangential component is not zero. The tangential component is calculated by using Neumann condition, $u' = v' = 0$. Therefore, we allow flow at the boundary but not the one that is parallel to the wall.

The implementation of open boundary is presented in Table 2.2 and Figure 2.8 in which n is a normal component of derivatives. On the right boundary, we implement persistent flux boundary in which the value at boundary is extrapolated linearly from values on two previous grids. Therefore, we can have the value at the boundary which is defined by,

$$\mathbf{b}_{N,j} = 2\mathbf{b}_{N-1,j} - \mathbf{b}_{N-2,j},$$

where $\mathbf{b}$ is a variable and N is the final grid at the right boundary. Using this type of boundary, we want to test out our hypothesis regarding the positive feedbacks loop that generate the vegetation "feather" pattern. As the water is flowing out of the system, the overall amount of water available in the system will be less than the previous case. Therefore, we hypothesize the recolonization of bare soil will be more difficult than periodic boundary case.

TABLE 2.2: Implementation of boundary conditions to all four boundaries in open boundary scenario.

Variable	**Boundary Conditions**			
	Top	**Bottom**	**Left**	**Right**
p	$\frac{dp}{dn} = 0$	$\frac{dp}{dn} = 0$	$\frac{dp}{dn} = 0$	Persistent Flux
w	$\frac{dw}{dn} = 0$	$\frac{dw}{dn} = 0$	$\frac{dw}{dn} = 0$	Persistent Flux
h	$\frac{dh}{dn} = 0$	$\frac{dh}{dn} = 0$	$\frac{dh}{dn} = 0$	$\frac{dh}{dn} = 0$
u	$\frac{du}{dn} = 0$	$\frac{du}{dn} = 0$	$u = 0$	$\frac{du}{dn} = 0$
v	$v = 0$	$v = 0$	$\frac{dv}{dn} = 0$	$\frac{dv}{dn} = 0$
z	$\frac{dz}{dn} = 0$	$\frac{dz}{dn} = 0$	$\frac{dz}{dn} = 0$	Persistent Flux

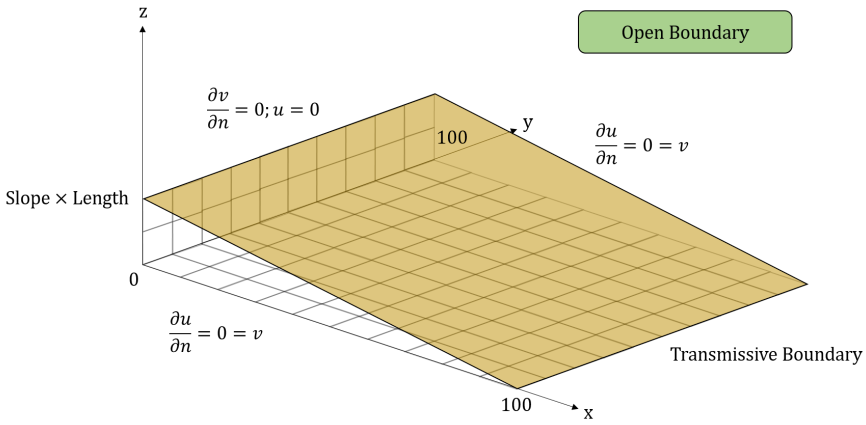

FIGURE 2.8: An illustration to open boundary condition. Both lateral and up-slope boundaries are limited by a wall (no-flow boundary), therefore we impose a combination of Dirichlet boundary and Neumann boundary conditions. On the down-slope boundary, we impose transmissive flow boundary which allows the matters to go out of the system.

Chapter 3

Results

In this chapter, we present our simulation results which are produced by implementing the finite difference method. In the first part of the chapter, we provide the pattern formation and the analysis of vegetation bands in preserving the slope gradient. After that, we will present the scenarios based on the explanation in the previous chapter. Lastly, the simulation results with open boundary are presented as a glimpse step for further research.

3.1 Pattern Formation

In this section, we present the first simulation results which contain vegetation density (p), surface water level (h), and topography dynamics (z) at 4000, 12000, and 20000 seconds which represents about six years of simulation time. The result can be seen in Figure 3.1. As can be seen in the figure, vegetation bands are established in topography with 0.25% of slope gradient. The topography allows water flow goes from the up-slope (left boundary) to the down-slope (right boundary). Vegetation bands orientation is perpendicular to the slope. Moreover, the vegetation on the up-slope band is denser than the one on the down-slope due to more abundant of water resources at the top of the bands. This condition also results in the up-slope movement of vegetation banded patterns. Furthermore, topography evolution are not changing much since soil erosion is prevented by vegetation bands.

3.1.1 Cross-sectional Area

To analyze the pattern, we take a closer look into the cross sectional area. Cross sectional area is taken by plotting the value of vegetation density or any variable along one of the axes. In this case, we present the cross sectional area along x-axis because it is a same direction as the water flow (see Figure 3.2). We plot the vegetation density along the axis and pick two peaks of vegetation density to look at closer into vegetated and bare soil areas. Taking a closer look to the cross-sectional areas, we can see an accumulation of water happened in the bare soil areas because of the low infiltration (see Figure 3.3). As the water level increases, the flow velocity becomes faster, and then it allows more erosion in the areas (see Figure 3.3a). On the other hand, in the vegetation patches, the water flow and water level are decreasing due to water infiltration and vegetation friction. Furthermore, as the vegetation bands are moving up-slope, the position of high soil erosion is shifting dependent on the speed of migration. As soon as the soil eroded, it creates a small depression which collect more water and facilitate vegetation to move up-slope faster. Therefore, we can find vegetation inhabit the depressions in the topography (see Figure 3.3b).

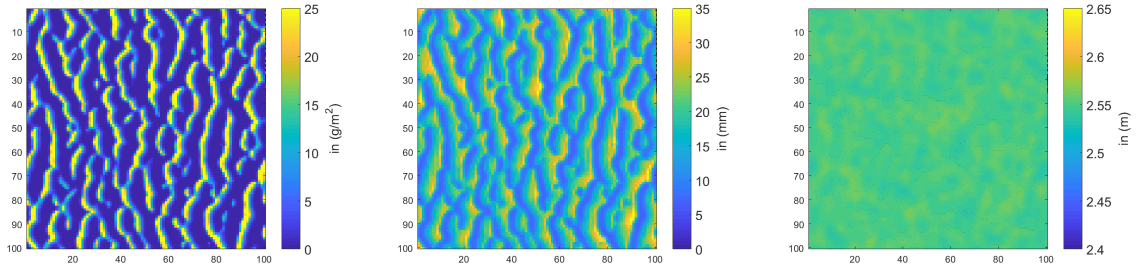

(A) After 4000 seconds

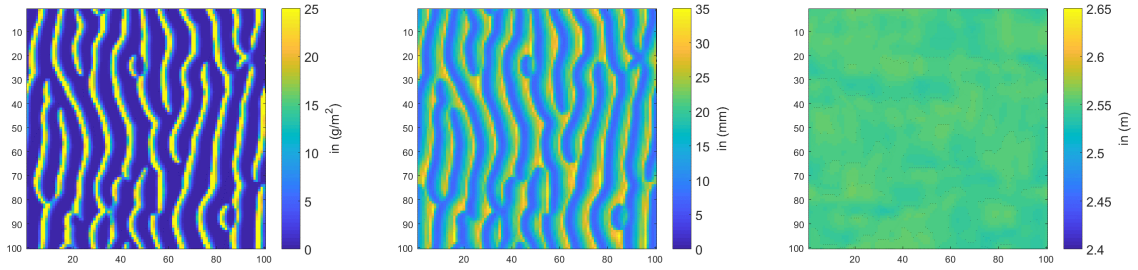

(B) After 12000 seconds

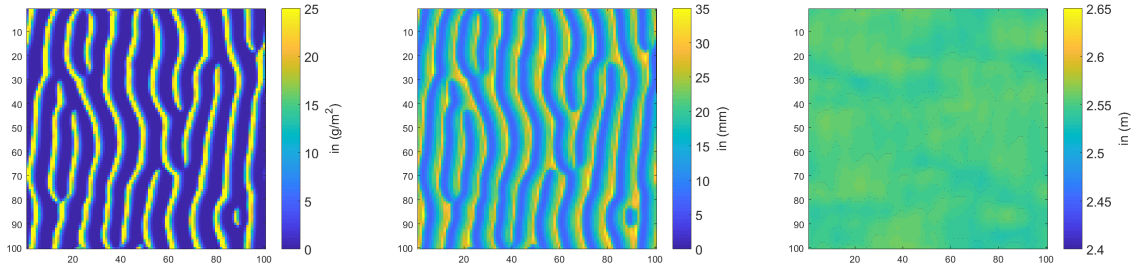

(C) After 20000 seconds

FIGURE 3.1: Numerical results with rainfall 1.0 mm per day showing vegetation banded patterns are formed thereby preventing soil erosion and channelization process. Color maps for vegetation ranging between 0-25 g^2/m, surface water level 0-35 mm, and bed topography 2.4 - 2.65 m.

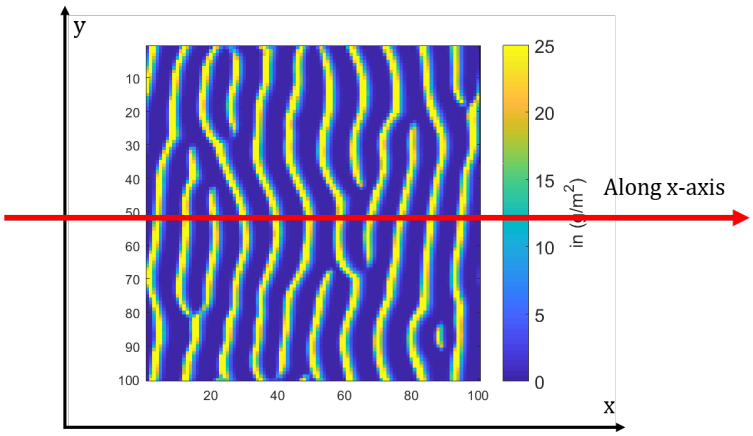

FIGURE 3.2: An illustration of cross-sectioning areas along x-axis.

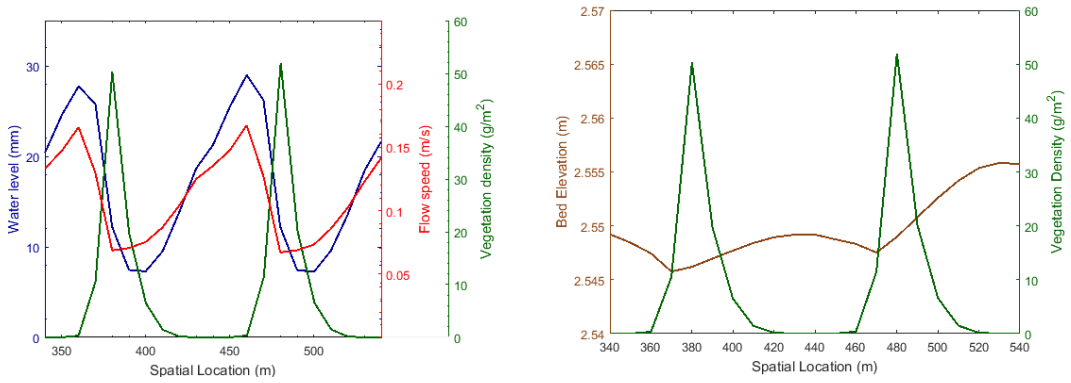

(A) (B)

FIGURE 3.3: Cross sectional areas results along x-axis with two different vegetation patches (a spatial location between 350 and 550 meters). (**A**) is a plot of surface water level (blue), flow field (red) and vegetation density (green) while (**B**) represent vegetation density (green) and topography dynamics (brown).

3.1.2 Vegetation-Topography: Slope Preservation

Bare soil areas allow high soil erosion due to high water flow speed and water column whereas vegetation patches prevent further erosion through friction loss. Because of vegetation bands are already established, soil erosion cannot deepen the channels further thereby sustaining the current physical topography. However, in case of no vegetation presence, the soil erosion creates topography variation in the areas. To quantify the difference in both simulation results, we compute the standard deviation of bed topography as a function of simulation time. We begin at the same value of standard deviation, i.e. around 0.03 meter. As the simulations are running over time, we found that the standard deviation of the simulation with vegetation is decreasing as the topography begin to reach its equilibrium while the other is increasing due to the channels deepening further (see Figure 3.4). Therefore, our finding suggests that vegetation bands preserve the slope of topography.

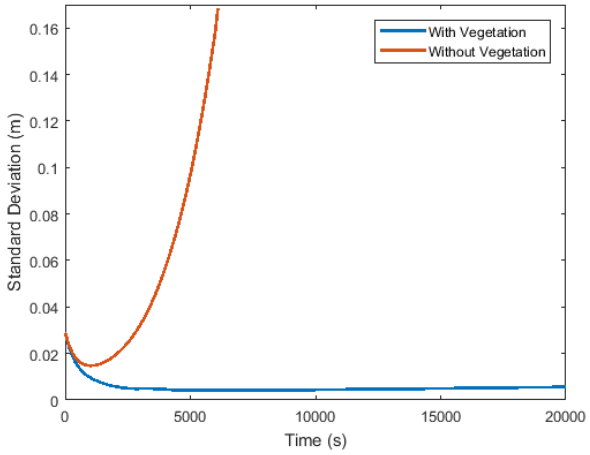

FIGURE 3.4: The standard deviation of bed elevation shows how vegetation keeps the slope gradient stable after several iterations. Red line represents the simulation without vegetation while the blue represents the simulation with vegetation. The standard deviation of the simulation without vegetation is presented until 6200 seconds of simulation time due to numerical instability.

3.2 Scenarios

Here in this section, we provide the numerical simulation results of each scenario. Land degradation scenario results are presented at the beginning of the section. We also present the comparison between the results and in case of no erosion involved. After that, we present the simulation results of vegetation colonization. A bifurcation diagram is presented at each scenario as an indicator of steady state solutions shift as the parameter changes. We also provide the periodogram of patterns concerning each scenario. Finally, we show the analysis of arced bands at the end of the section.

3.2.1 Scenario 1: Land Degradation

In the scenario of land degradation, we start with the initial parameters presented in table 2.1 with rainfall parameter is equals to 1 mm/day. The setup results in the pattern in Figure 3.1. The spatial averaged vegetation density of this pattern is around 8 g/mm^2 (see point 1 at Figure 3.5). As the rainfall decreases (0.05 mm/day on each step), we can see that the average biomass is declining linearly. However, at point 2 in the same graph, the linear decrease begin to decelerate as the vegetation bands are breaking apart (see Figure 3.6b). This condition leads to a lower pattern wavelength. Because of vegetation bands begin to retract into shorter stripes, it allows soil erosion to take place in between patches. Soil erosion creates topographic depression and channels which help vegetation to collect water (see Figure 3.6c). Therefore, vegetation patches still can survive even though in the condition of low rainfall.

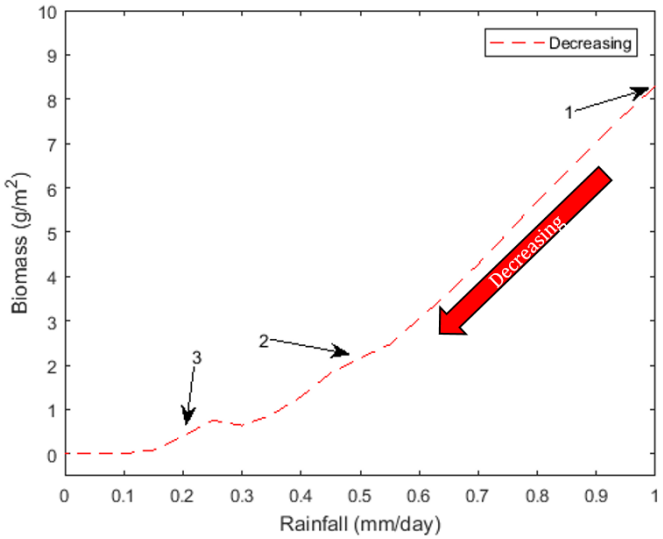

FIGURE 3.5: Spatially averaged biomass (on y-axis) as a function of rainfall (on x-axis). The average values of vegetation density are declining as rainfall decreases. Point 1, 2, and 3 represent the average biomass at rainfall parameters 1, 0.5, and 0.2 mm/day, respectively.

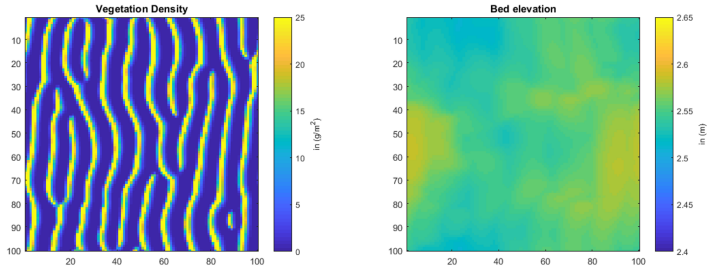

(A) Point 1

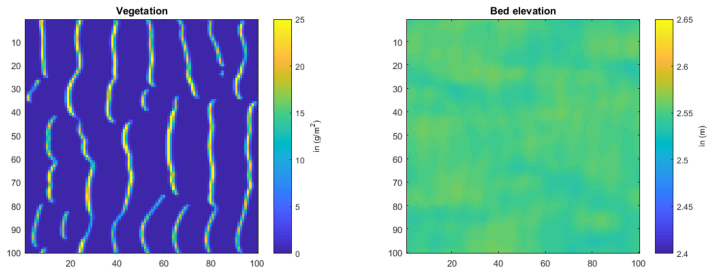

(B) Point 2

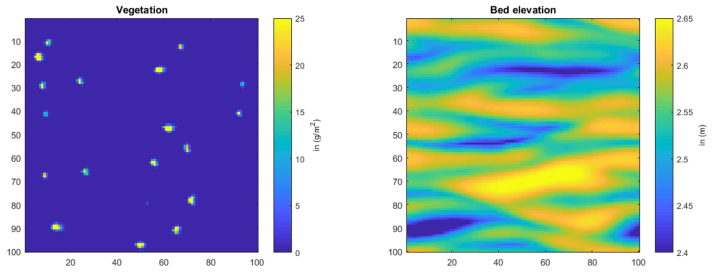

(C) Point 3

FIGURE 3.6: The evolution of vegetation pattern and topography as the rainfall is decreasing. Figure (**A**) represents an established vegetation banded pattern while Figure (**B**) represents the patterns breaking up condition as the rainfall is getting lower. In Figure (**C**), vegetation patches remain to exist in the system due to the channels and depressions facilitation.

With vs Without Erosion

In this study, we compare the simulation if there is no soil erosion involved in the system (erodible bed is unchanged). The result can be found in Figure 3.7. The averaged biomass is about the same which is notified by almost coincided lines. At an interval between 0.15-0.35 mm/day, the simulation results show the influence of topography variance to the vegetation patches. Vegetation patches in without erosion simulation (blue line) are already extinct as the rainfall below 0.3 mm/day whereas in the other simulation (red line) vegetation patches are still present and survive due to the channels and depressions presence. The topographic variations in the simulation facilitate vegetation in concentrating water. Therefore, vegetation patches can grow in the valley of the channels and topographic depressions while the flat erodible bed cannot support the growth of vegetation patches any longer.

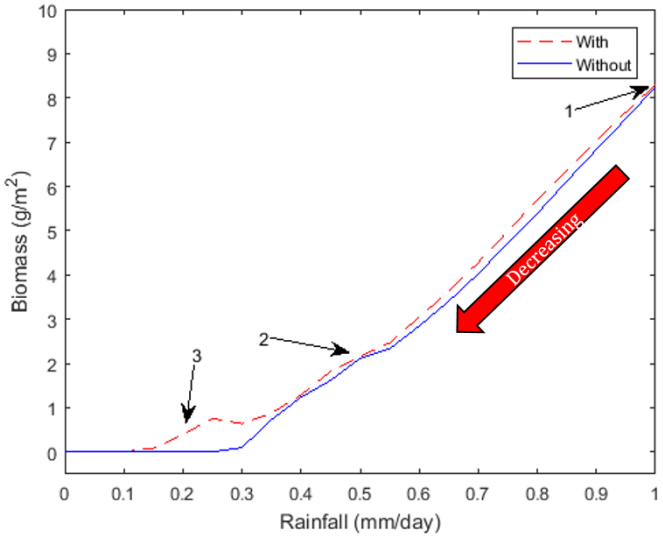

FIGURE 3.7: Comparison of averaged vegetation density as a function of rainfall between the simulations with and without erosion in case of decreasing rainfall. The solid blue line represents the simulation without erosion while the dashed red line represents the simulation with erosion.

Spectral Analysis

Here we provide the analysis of vegetation banded patterns by using the spectral analysis method. The method can show the characteristic of the pattern in the form of wavelength and the pattern orientation. The results can be seen in Figure 3.8. Firstly, we can see in the periodogram (upper right), there are two solid dots inversely mirroring to the center (blue dots). These two dots represent the peak of our data which produce a same variance. The distance from the center to one of either peaks is the same and represents the wave number while the orientation of the pattern can be seen from the position of the two peaks. As shown in the radial spectrum, the wave number of our pattern is around ten which indicate ten bands found in the pattern. This result correlates to the wavelength of 100 meters between two vegetation bands. Meanwhile, in the angular spectrum, it shows the orientations of the pattern are mostly found in an interval of angle between 90-110 degrees. This result corresponds to the pattern which is perpendicular to the slope.

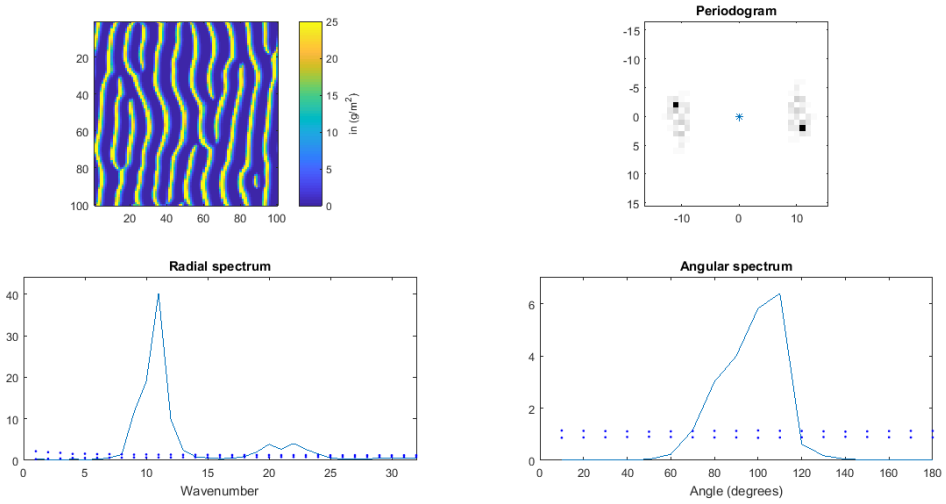

FIGURE 3.8: The spectral analysis of vegetation banded pattern. The periodogram (upper right) shows two peaks of data variance and the orientation of the pattern while radial (bottom left) and angular spectrum (bottom right) count the spectrum which corresponds to each frequency and angle, respectively.

3.2.2 Scenario 2: Vegetation Colonization

In this section, we simulate the colonization of bare soil by vegetation patches as described in 2.3.4. The result can be seen in Figure 3.9. In a long dry period, which is at an interval of rainfall between 0-0.2 mm/day, the uniform non-vegetated steady state solution is stable. As soon as the channels are formed (see Figure 3.10c), vegetation colonize the valleys due to higher amount of water available than in the ridges. Because of vegetation presence in the channels, it suppresses the soil erosion. Furthermore, as the rainfall increases, vegetation "arcs" are developed and the channels begin to transform into topographic depressions (see Figure 3.10b). Finally, at 1 mm/day rainfall, these topographic depressions are reshaping vegetation bands from "stripes" into "arcs" (see Figure 3.10a).

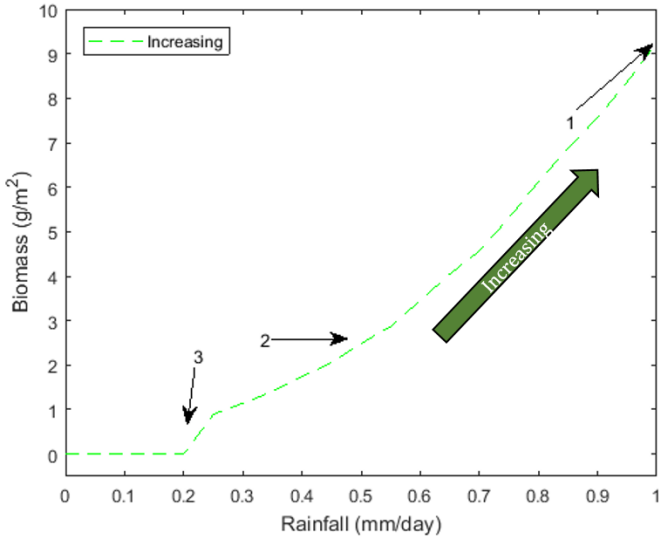

FIGURE 3.9: Spatially averaged biomass (on y-axis) as a function of rainfall (on x-axis). The average values of vegetation density are improving as rainfall increases. Point 1, 2, and 3 represent the average biomass at rainfall parameters 1, 0.5, and 0.2 mm/day, respectively.

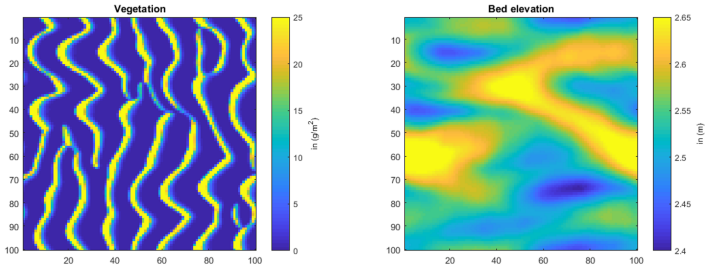

(A) Point 1

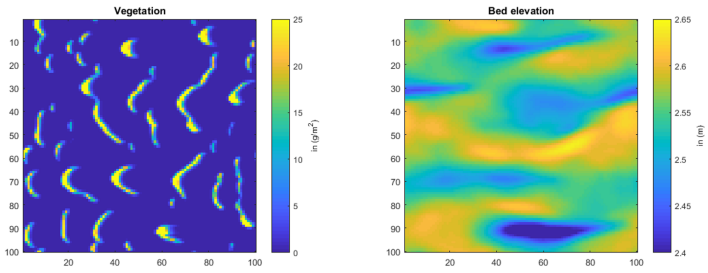

(B) Point 2

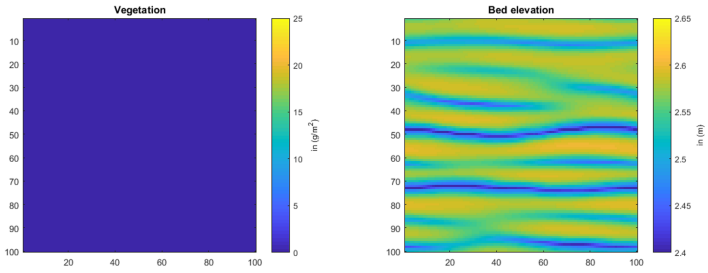

(C) Point 3

FIGURE 3.10: The evolution of vegetation pattern and topography as the rainfall is increasing. In Figure (**C**), a non-vegetated state remains stable while the topographic variation is already developed. Figure (**B**) represents vegetation arcs and topographic depressions emergence in the system while Figure (**A**) represents an established vegetation "arced" band pattern.

With vs Without Erosion

Using the same setup as described in the previous section, here we provide the simulation results of with and without erosion modeling. The result can be seen in Figure 3.11. The same conclusion can be taken from previous result that at an interval 0.2-0.3 mm/day, topographic variation promotes vegetation to recover faster than a flat topography. In the simulation without soil erosion, the colonization begin to appear after 0.3 mm/day whereas in the simulation with soil erosion, as the channels have been formed at 0.2 mm/day, the recovery starts sooner. At the rainfall 1 mm/day simulation, the average vegetation density is slightly higher than the previous simulation which is about 9 g/m^2.

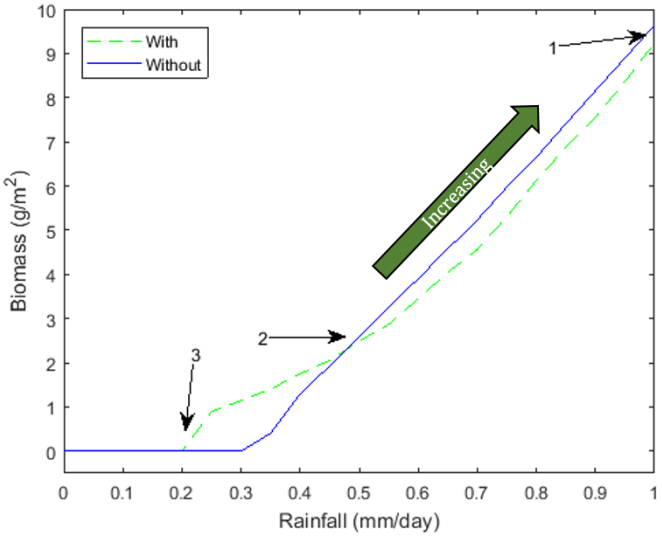

FIGURE 3.11: Comparison of averaged vegetation density as a function of rainfall between the simulations with and without erosion in case of increasing rainfall. The solid blue line represents the simulation without erosion while the dashed green line represents the simulation with erosion.

Spectral Analysis

Comparing the pattern resulted in this section to the pattern in Figure 3.1, the "arced" bands indicate multiple different orientations of patterns due to the topographic variation. Here in this section, we provide the analysis of the pattern orientation and wavelength in case of vegetation colonization. Firstly, we can see the periodogram at the upper right of Figure 3.12. The periodogram shows that there are multiple peaks or at least four peaks can be seen clearly on the data variance. These peaks are represented in the angular spectrum (bottom right) which shows two high spectrum of pattern orientations, i.e. 70 degree and 100 degree with respect to the y-axis in a clockwise direction. Corresponding angles are associated with the direction of the arcing vegetation bands. On the other hand, the radial spectrum shows a high spectrum at wave number seven in the pattern. This result correlates to the wavelength of about 142 meters.

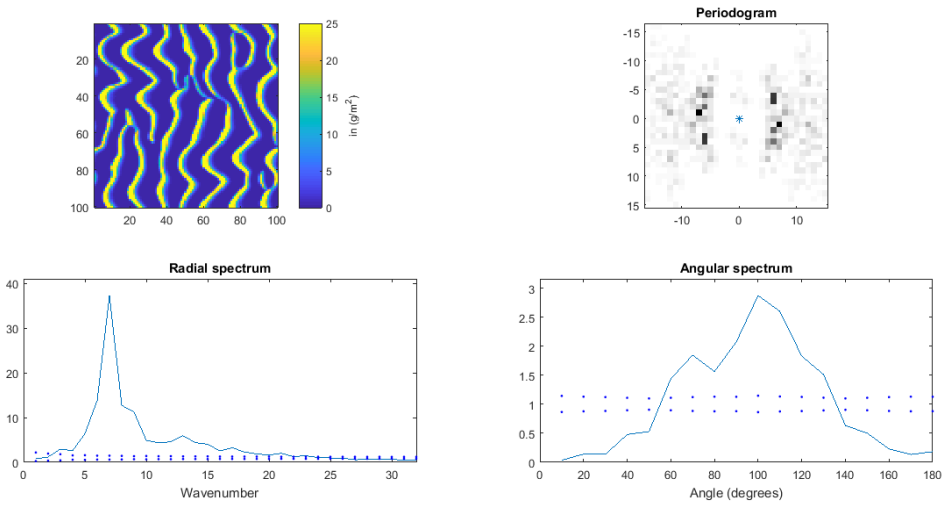

FIGURE 3.12: The spectral analysis of vegetation "arced" bands pattern. The periodogram shows multiple peaks which correspond to multiple directions of patterning while the distances between the peaks and the center represent the wave number found in the result.

Arced Bands: An Indicator of Ecosystems Recovery

Vegetation banded patterns can emerge from both land degradation and vegetation colonization scenarios, but only one can generate "arc" bands. In vegetation colonization scenario, we have shown that vegetation "arced" bands occur in the system due to the presence of topographic variation (see Figure 3.13b) whereas in the simulation without erosion (see Figure 3.13d), vegetation bands appear to be more straight and have a higher wavelength. These two findings indicate that if the topographic variation develops quickly during a long dry period, "arced" bands will occur in the system due to non-uniform water distribution. Otherwise, vegetation "straight" bands will prevent the soil erosion and create a topography which only allows uniform lateral water flow. Moreover, the soil erosion prevention also helps vegetation "arced" bands to erase and transform channels into topographic depressions in the system (see Figure 3.10a). In other words, vegetation "arced" bands can only emerge in a condition which is possible to develop topography variance in the first place, otherwise "straight" bands will dominate the pattern. Therefore, our findings suggest that vegetation "arced" bands can be an indicator of ecosystems that are recovering from shallow drainage patterns or degraded lands.

In this study, we also found that vegetation bands are aligned to the topography contour lines. All four patterns that we have in the simulation results agree with this condition. The results can be seen in Figure 3.13. In case of straight vegetation bands (see Picture (**A**), (**C**) and , (**D**)), the contour lines (in red line) are in the same direction as vegetation bands. Meanwhile in case of vegetation "arced" bands (see Picture (**B**)), the topography contour lines are reflected by the arcing direction of vegetation bands due to vegetation growth differences between vegetation in the valleys and on the ridges. The variation of growth rate happens because of more water available in the valleys than on the ridges thereby increasing vegetation growth rate in the valleys. This condition allows vegetation bands to "travel" upslope faster compared to the one which grow on the ridges. Therefore, these traveling speed differences create an effect of arcing direction which is aligned to the topography contour.

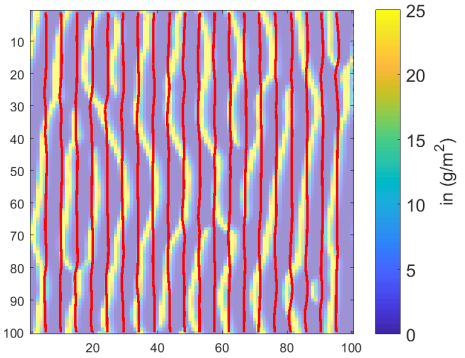

(A) Vegetation "straight" bands as a result of land degradation simulation.

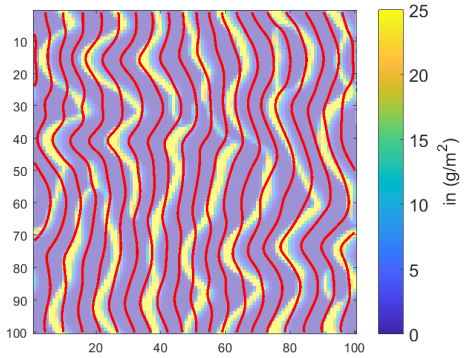

(B) Vegetation "arced" bands as a result of vegetation colonization simulation.

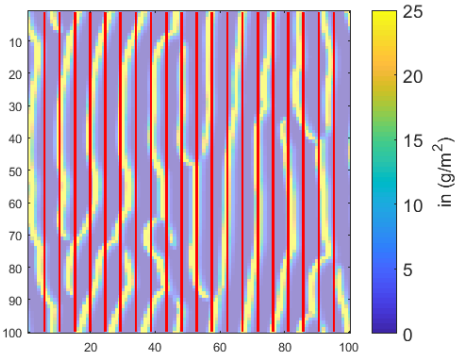

(C) Vegetation "straight" bands as a result of land degradation simulation (without erosion).

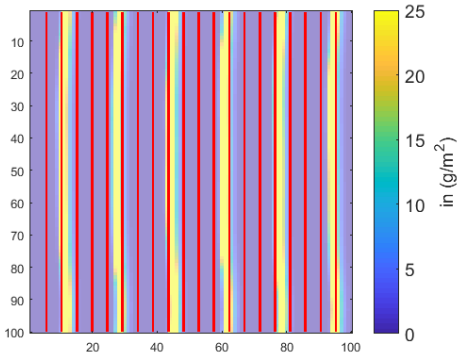

(D) Vegetation "straight" bands as a result of vegetation colonization simulation (without erosion).

FIGURE 3.13: The plot of topography contour (red line) in the same frame with vegetation bands (yellow bands). All four cases of vegetation patterns are aligned to the topography contour.

3.2.3 Scenario 3: Open Boundary Condition

Boundary condition plays a crucial role in determining the exchange of matters from and into the system besides local external/internal forces. Previous scenarios implement the periodic boundary condition in which matter cannot go out of the system through boundaries. Therefore, vegetation bands can sustain in the domain and prevent further soil erosion. However, in an open boundary condition, the up-slope movement of vegetation can lead to the creation of channels at the down-slope. The absence of negative response to the soil erosion leads to channels deepening. The result can be seen in Figure 3.14. Other attempts, for example changing parameters and other type of open boundary, have been made but still produced inconclusive results.

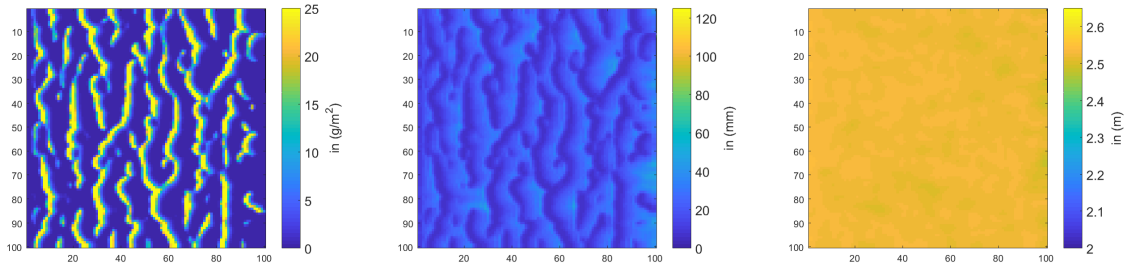

(A) After 3000 seconds

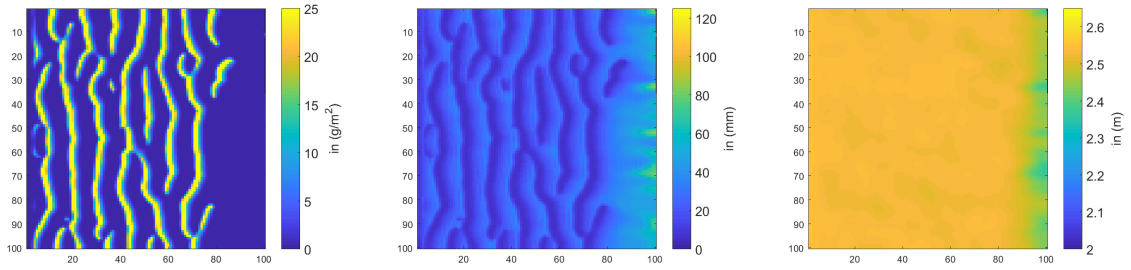

(B) After 8000 seconds

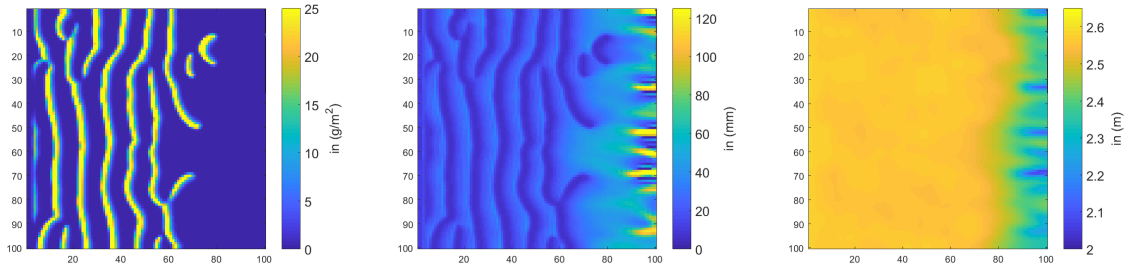

(C) After 12000 seconds

FIGURE 3.14: Numerical results with rainfall 1.0 mm per day showing vegetation banded patterns are leaving out of the system which lead to channels incision down-slope. Color maps for vegetation ranging between 0-25 g^2/m, surface water level 0-120 mm, and bed topography 2 - 2.65 m. Because of numerical instability in the simulation, we only provide the result until 12000 simulation time.

Chapter 4

Conclusion and Discussion

4.1 Summary and Conclusion

In this study, we have developed an extended version of Rietkerk model which can provide better information in capturing the impact of topography variation on hydrodynamics and vegetation patterning. The current surface water modeling can generate non-uniform water flow which allows topography variation through soil erosion. The results show the emergence of vegetation "arced" bands as a result of a non-uniform distribution of water and topography variation. The soil erosion modeling, however, is still limited in representing the real physical process. Although it already includes the positive response of water flow velocity, the erosion process here is described as evaporated soil instead of transported soil by water flow. In the real physical process, eroded soil is transported through the water column to another cell. Further studies should include a better representation of soil erosion modeling to generate more realistic simulations. Regardless, our modeling study suggests the consideration to include topography variation into the model as it influences vegetation patterning.

Vegetation feedback to topography dynamics is a key in the widely observed gently sloped landscapes in arid ecosystems. Using the proposed mathematical model, we compared the effects of the presence and absence of vegetation bands on topography evolution. When vegetation bands exist in a gently sloped landscape, the physical topography of the landscape is preserved through soil erosion prevention. The transverse vegetation bands act as a natural "bench" to reduce water flow velocity in the system which then decreases the amount of eroded soil. Moreover, as the flow velocity is reduced, water columns are building-up at the up-slope part of the bands which then infiltrate more water thereby sustaining the presence of vegetation bands. On the other hand, in the absence of vegetation bands, channels incision begin to appear as the water flow velocity increases over time. Therefore, topographic variation is unavoidable since there is no negative response to stop the erosion process. The counteract feedback in this study, however, only include the vegetation friction which reduces the water flow velocity. It is also possible for future studies, to consider the root catchment of vegetation as it diminishes soil erodibility. Thus, we conclude that the presence of vegetation bands in arid ecosystems preserve the current physical topography of the landscape by preventing soil erosion through vegetation friction.

In scenarios of environmental changes, vegetation has an extra advantage in the existence of topographic variation. In this study, we set up two scenarios which simulating the change in rainfall patterns, i.e., decreasing (land degradation) and increasing (vegetation colonization) amount of rains. Each scenario is compared to the condition in which the topographic variation is negligible. The simulation results showed that topographic variation increases the resilience of vegetation in arid ecosystems through resisting degradation and faster recovery. The underlying topographic variation such as channels and depressions facilitate vegetation growth by concentrating water. Therefore, in a low rainfall condition, vegetation still survives in the system by growing on top of the depressions or channels.

Correspondingly, vegetation recover from degraded state faster in the presence of topographic variation than a flat topography since the depressions and channels accumulate water that is beneficial for vegetation growth. However, the simulations used an estimated value of parameters and a method of a morphological factor which may overestimate the impact of hydrodynamics on the vegetation growth and topography evolution. We suggest in further study to consider a more reliable estimate by comparing to the real observation or using a combination of pseudo-transient method and GPU computing to achieve an efficient and fast computation. Nevertheless, our results confirm the negative feedback hypothesis in which channels and depressions facilitate vegetation to grow thereby increasing the resilience of vegetation in arid ecosystems.

4.2 Discussion

We found that the feedback between vegetation loss and soil erosion leads to heterogeneity of topography landscapes that allows vegetation to persist or re-establish after severe drought thereby increasing the resilience of arid ecosystems. As the environmental condition is getting worse, which is notified by fewer rains, vegetation bands start to break-up, and soil erosion reshapes the landscape topography to create water ponds or lanes. Then, these ponds become temporary water reserves for vegetation to survive in harsh conditions. In other cases, shallow water channels and depressions can emerge during a long dry period thereby allowing water accumulation. This condition leads to a quick re-establishment of vegetation in the depressions and channels since the topography variation facilitates vegetation in redistributing water flow thereby enhancing the growth rate.

In Rietkerk et al., 2004, decreased rainfall can lead to a sudden shift from a vegetated state into a degraded state due to the loss of vegetation water-harvesting mechanisms. Increased soil erosion along with degradation, however, can enhance topographic variation, for example, depressions and shallow channels which can concentrate water after rains. The accumulation of water allows vegetation to re-establish in the depressions thereby preventing the ecosystem collapse abruptly. Correspondingly, increased rainfall in bare soil state may recover quicker than it was suggested because of topographic variation facilitates vegetation in concentrating water. Therefore, future studies might then need to consider the feedbacks between vegetation and topography since both feedbacks influence each other which can alter their response to environmental changes.

Our works agree with a recently published observational study by Gowda, Iams, and Silber, 2018 that vegetation "arced" bands widen even in a condition with steep increases of human activities. Bands widening in these areas may appear due to undisturbed shallow depressions in creating water accumulation even though the bare soil between bands are used as roads and dirt tracks. The results would be different in a case with significant changes in land use, for example, new settlements or agriculture. Undulating valleys may be transformed into houses or farms which reduce its natural purpose in accumulating water after rains. Therefore, we argue that vegetation and topography feedbacks can increase the resilience of vegetation in arid ecosystems.

Vegetation patterns are closely related to its origin whether it comes from a stability change in decreased rainfall or vegetation colonization of bare soil. The two different origins have been suggested to be possible because of the presence of different wavelength found in the system (Sherratt, 2015). Our results have shown that vegetation "arced" bands can only appear in a condition which topography variation present in the first place then it evolves during continuous rains. After the bands are fully intact, vegetation seems to preserve the slope gradient of landscapes which agree with largely observed patterns which only appear at a certain interval of slope (Deblauwe et al., 2011). These findings suggest

that the observed vegetation "arced" bands in arid ecosystems can be an indicator of systems that are recovering from shallow drainage lines. Further studies may need to have empirical data which shows the origin of vegetation pattern in the ecosystem.

Positive feedback hypothesis is still arguable and open for further studies. Our attempts to confirming the positive feedback hypothesis by imposing the open boundary condition still produce an inconclusive result. Vegetation up-slope movement leads to channels incision at the down-slope boundary instead of water concentrating "competition" between channels and vegetation. One of a possible reason is the steepness of the slope. When it is steep enough to allow drainage lines, vegetation patterns can break-up which causes channels deepening (Saco and Moreno-De Las Heras, 2013). Deeper channels do not allow vegetation bands to grow because the slope is too steep to hold sheet water flow causing ecosystem collapse. Moreover, the possibility of alternative global bistability between vegetation bands pattern and feather pattern is still unexplored even though the recent picture of Macfadyen, 1950 (see Figure 1.3) strongly suggest both condition are stable. Further modeling studies are needed to investigate this possibility since soil erosion may worsen the effect of being in a degraded state and make ecosystem recovery even more difficult.

We have provided new investigation results suggesting vegetation and topography feedbacks play a crucial role in vegetation patterning and topography evolution and we argue that when negative vegetation response to soil erosion dominates the system, topography variation facilitates vegetation growth thereby increasing the resilience of arid ecosystems. However, negative topography response domination remains partly unexplored in which deep drainage lines may be created. The condition keeps further studies to be recommended and open to promoting mathematical modeling combined with observational studies in ecosystem management.

Appendix A

Derivation of the Model

Here we provide the derivation of homogeneous steady state solutions. General solution of homogeneous steady state solutions are achieved but we implemented a special case of uniform degraded state for the initial conditions.

A.1 Homogeneous Steady State Derivation

Homogeneous steady state condition is reached when all the variables in the system are unchanged after several steps of iterations in time. In other words, we could assume homogeneous steady state occurs when $\frac{\partial p}{\partial t} = \frac{\partial h}{\partial t} = \frac{\partial w}{\partial t} = \frac{\partial u}{\partial t} = \frac{\partial v}{\partial t} = \frac{\partial z}{\partial t} = 0$. Then by using this assumption we can compute the homogeneous steady state condition as follows,
Vegetation Steady State

$$\text{Biomass Dynamics} \rightarrow [\text{Growth}] - [\text{Death}] + [\text{Seeds Dispersal}]$$

$$\frac{\partial p}{\partial t} = cg_{max}\frac{w}{w + k_1}p - dp + D_p\Delta p$$

$$0 = cg_{max}\frac{\bar{w}}{\bar{w} + k_1}\bar{p} - d\bar{p} + D_p\Delta\bar{p}$$

Because it is homogeneous, then all the derivative in space are equal to zero. Therefore, we can have

$$0 = cg_{max}\frac{\bar{w}}{\bar{w} + k_1}\bar{p} - d\bar{p}$$

$$0 = \left(cg_{max}\frac{\bar{w}}{\bar{w} + k_1} - d\right)\bar{p}$$

From this equation we found that there are two options,

$$0 = cg_{max}\frac{\bar{w}}{\bar{w} + k_1} - d \text{ or } \bar{p} = 0$$

First let us focus on steady state in which all variables are exist (non-zero). Then we can have,

$$\begin{aligned} d &= cg_{max}\frac{\bar{w}}{\bar{w}+k_1} \\ d(\bar{w}+k_1) &= cg_{max}\bar{w} \\ d\bar{w}+dk_1 &= cg_{max}\bar{w} \\ d\bar{w}-cg_{max}\bar{w} &= -dk_1 \\ \bar{w} &= \frac{-dk_1}{d-cg_{max}} \\ \bar{w} &= \frac{dk_1}{cg_{max}-d} \end{aligned} \tag{A.1}$$

Then the next computation comes from the second equation,
Surface Water Steady State

$$\text{Local Water Height Dynamic} + \text{Net Flux} \rightarrow [\text{Rainfall}] - [\text{Infiltration}]$$

$$\begin{aligned} \frac{\partial h}{\partial t}+\frac{\partial (hu)}{\partial x}+\frac{\partial (hv)}{\partial y} &= R-\alpha h\frac{p+k_2w_0}{p+k_2} \\ 0+\frac{\partial (\bar{h}\bar{u})}{\partial x}+\frac{\partial (\bar{h}\bar{v})}{\partial y} &= R-\alpha \bar{h}\frac{\bar{p}+k_2w_0}{\bar{p}+k_2} \end{aligned}$$

Using same treatment as in the previous equation, we can have,

$$\begin{aligned} 0 &= R-\alpha \bar{h}\frac{\bar{p}+k_2w_0}{\bar{p}+k_2} \\ -R &= -\alpha \bar{h}\frac{\bar{p}+k_2w_0}{\bar{p}+k_2} \\ \alpha \bar{h}(\bar{p}+k_2w_0) &= R(\bar{p}+k_2) \\ \bar{h} &= \frac{R(\bar{p}+k_2)}{\alpha(\bar{p}+k_2w_0)} \end{aligned} \tag{A.2}$$

After we have gotten the expression of the equilibrium for the two variables, we can continue to the third equation,
Soil Water Steady State

$$\text{Soil Water} \rightarrow [\text{Infiltration}] - [\text{Water-uptake}] - [\text{Evaporation}] + [\text{Water Movement}]$$

$$\begin{aligned} \frac{\partial w}{\partial t} &= \alpha h\frac{p+k_2w_0}{p+k_2}-g_{max}\frac{w}{w+k_1}p-r_ww+D_w\Delta w \\ 0 &= \alpha \bar{h}\frac{\bar{p}+k_2w_0}{\bar{p}+k_2}-g_{max}\frac{\bar{w}}{\bar{w}+k_1}\bar{p}-r_w\bar{w}+D_w\Delta \bar{w} \end{aligned}$$

Using same treatment as in the previous equation, we can have,

$$0 = \alpha \bar{h}\frac{\bar{p}+k_2w_0}{\bar{p}+k_2}-g_{max}\frac{\bar{w}}{\bar{w}+k_1}\bar{p}-r_w\bar{w}$$

Then substitute what we found in the previous computation, $\bar{h}$ to the equation A.2, we can have,

$$
\begin{aligned}
0 &= \alpha \frac{R(\bar{p}+k_2)}{\alpha(\bar{p}+k_2 w_0)} \frac{\bar{p}+k_2 w_0}{\bar{p}+k_2} - g_{max} \frac{\bar{w}}{\bar{w}+k_1} \bar{p} - r_w \bar{w} \\
0 &= \alpha \frac{R(\bar{p}+k_2)}{\alpha(\bar{p}+k_2 w_0)} \frac{\bar{p}+k_2 w_0}{\bar{p}+k_2} - g_{max} \frac{\bar{w}}{\bar{w}+k_1} \bar{p} - r_w \bar{w} \\
0 &= R - g_{max} \frac{\bar{w}}{\bar{w}+k_1} \bar{p} - r_w \bar{w} \\
g_{max} \frac{\bar{w}}{\bar{w}+k_1} \bar{p} &= R - r_w \bar{w} \\
\bar{p} &= (R - r_w \bar{w}) \left[\frac{\bar{w}+k_1}{g_{max} \bar{w}} \right]
\end{aligned} \tag{A.3}
$$

Furthermore, to get simpler expressions of the steady state, we can substitute $\bar{w}$ to the equation of $\bar{p}$ and $\bar{h}$. So that we can have,

$$
\begin{aligned}
\bar{p} &= \left(R - r_w \frac{dk_1}{cg_{max} - d} \right) \left[\frac{\frac{dk_1}{cg_{max}-d} + k_1}{g_{max} \frac{dk_1}{cg_{max}-d}} \right] \\
\bar{p} &= \left(R - r_w \frac{dk_1}{cg_{max} - d} \right) \left[\frac{d + cg_{max} - d}{g_{max} d} \right] \\
\bar{p} &= \left(R - r_w \frac{dk_1}{cg_{max} - d} \right) \frac{c}{d} \\
\bar{p} &= \frac{Rc}{d} - \frac{r_w c k_1}{cg_{max} - d}
\end{aligned} \tag{A.4}
$$

On the other hand, for the surface water, we can have,

$$
\bar{h} = \frac{R(\frac{Rc}{d} - \frac{r_w c k_1}{cg_{max}-d} + k_2)}{\alpha(\frac{Rc}{d} - \frac{r_w c k_1}{cg_{max}-d} + k_2 w_0)} \tag{A.5}
$$

Thus, the three equations A.1, A.4, and A.5 are the parameter-based expression of the homogeneous steady state condition for our system.

Furthermore, if we look at the momentum equation,

Momentum Equation

$$
\text{Local Inertia} + \text{Conv. Acc.} \rightarrow -[\text{Pressure}] - [\text{Friction Loss}] + [\text{Turbulent}]
$$

$$
\begin{aligned}
\frac{\partial u}{\partial t} + u \frac{\partial u}{\partial x} + v \frac{\partial u}{\partial y} &= -g \left(\frac{\partial (h + z + z_{ref})}{\partial x} \right) - S_{fx} + D_u \Delta u \\
\frac{\partial v}{\partial t} + u \frac{\partial v}{\partial x} + v \frac{\partial v}{\partial y} &= -g \left(\frac{\partial (h + z)}{\partial y} \right) - S_{fy} + D_v \Delta v
\end{aligned}
$$

with the friction function can defined as,

$$
\begin{aligned}
S_{fx} &= \frac{g}{C^2 h} u \sqrt{u^2 + v^2} \\
S_{fy} &= \frac{g}{C^2 h} v \sqrt{u^2 + v^2}
\end{aligned}
$$

We can develop the homogeneous steady state by looking at one of the equations and the other will follow. For example in x-direction, we have

$$\frac{\partial u}{\partial t} + u\frac{\partial u}{\partial x} + v\frac{\partial u}{\partial y} = -g\left(\frac{\partial(h+z+z_{ref})}{\partial x}\right) - S_{fx} + D_u\Delta u$$

As our system goes to steady state condition and homogeneous, then we have $\frac{\partial u}{\partial t} = \frac{\partial u}{\partial x} = \frac{\partial u}{\partial y} = \frac{\partial(h+z+z_{ref})}{\partial x} = \Delta u = 0$. From that moment, the equation becomes,

$$\begin{aligned} 0 &= -S_{fx} \\ 0 &= \frac{g}{C^2\bar{h}}\bar{u}\sqrt{\bar{u}^2+\bar{v}^2} \end{aligned}$$

Because $\frac{g}{C^2\bar{h}} \neq 0$ then $\bar{u}\sqrt{\bar{u}^2+\bar{v}^2} = 0$. Lets assume $\bar{u} \neq 0$. Then we have,

$$\begin{aligned} \sqrt{\bar{u}^2+\bar{v}^2} &= 0 \\ \bar{u}^2+\bar{v}^2 &= 0 \end{aligned}$$

From here, we know that $\bar{u}^2, \bar{v}^2 \geq 0$. So that the only solution to this equation is satisfied by $\bar{u} = 0$ and $\bar{v} = 0$. Thus, our first assumption is unreliable and then we found that the homogeneous steady state condition for water flow velocity are satisfied by $(\bar{u}, \bar{v}) = (0, 0)$.

General equations of non-trivial solution, that fulfills homogeneous steady state condition, are satisfied by equation A.1, A.4, and A.5. However, if we look at a specific case at $\bar{p} = 0$, then from A.3, we can have one steady state, $\bar{w} = \frac{R}{r_w}$ and $\bar{h} = \frac{R}{\alpha w_0}$. This steady state tell us that the system is in bare soil condition which has no vegetation grows in the system.

Bibliography

Adeel, Zafar et al. (2005). *Ecosystems and human well-being: desertification synthesis*. Tech. rep. World Resources Institute (WRI).

Baptist, M. J. et al. (2007). "On inducing equations for vegetation resistance". In: *Journal of Hydraulic Research* 45.4, pp. 435–450. ISSN: 00221686. DOI: 10.1080/00221686.2007.9521778.

Bastiaansen, Robbin et al. (2018). "Multistability of model and real dryland ecosystems through spatial self-organization". In: *Proceedings of the National Academy of Sciences* 115.44, p. 201804771. ISSN: 0027-8424. DOI: 10.1073/pnas.1804771115. URL: http://www.pnas.org/lookup/doi/10.1073/pnas.1804771115.

Couteron, P. and O. Lejeune (2001). "Periodic spotted patterns in semi-arid vegetation explained by a propagation-inhibition model". In: *Journal of Ecology* 89.4, pp. 616–628. ISSN: 00220477. DOI: 10.1046/j.0022-0477.2001.00588.x.

Deblauwe, Vincent et al. (2011). "Environmental modulation of self-organized periodic vegetation patterns in Sudan". In: *Ecography* 34.6, pp. 990–1001. ISSN: 09067590. DOI: 10.1111/j.1600-0587.2010.06694.x.

Gandhi, Punit et al. (2018). "A topographic mechanism for arcing of dryland vegetation bands". In: *Journal of The Royal Society Interface* 15.147, p. 20180508.

Gilad, E et al. (2004). "Ecosystem engineers: From pattern formation to habitat creation". In: *Physical Review Letters* 93.9, p. 98105. ISSN: 00319007. DOI: 10.1103/PhysRevLett.93.098105. URL: http://link.aps.org/doi/10.1103/PhysRevLett.93.098105.

Gowda, Karna, Sarah Iams, and Mary Silber (2018). "Signatures of human impact on self-organized vegetation in the Horn of Africa". In: *Scientific reports* 8.1, p. 3622.

Hardenberg, J. von et al. (2001). "Diversity of vegetation patterns and desertification". In: *Physical Review Letters* 87.19, pp. 198101–1–198101–4. ISSN: 10797114. DOI: 10.1103/PhysRevLett.87.198101.

Hendrix, Cullen S and Idean Salehyan (2012). "Climate change, rainfall, and social conflict in Africa". In: *Journal of peace research* 49.1, pp. 35–50.

HilleRisLambers, Reinier et al. (2001). "Vegetation Pattern Formation in Semi-Arid Grazing Systems". In: *Ecology* 82.1, pp. 50–61. ISSN: 00129658. DOI: 10.1890/0012-9658(2001)082[0050:VPFISA]2.0.CO;2. URL: http://www.jstor.org/stable/2680085.

Kämpf, Jochen (2009). *Ocean Modelling for Beginners: Using Open-Source Software*. Springer Science & Business Media.

Klausmeier, Christopher A. (1999). "Regular and irregular patterns in semiarid vegetation". In: *Science* 284.5421, pp. 1826–1828. ISSN: 00368075. DOI: 10.1126/science.284.5421.1826. URL: http://www.sciencemag.org/cgi/doi/10.1126/science.284.5421.1826.

Koppel, Johan van de et al. (2005). "Scale-Dependent Feedback and Regular Spatial Patterns in Young Mussel Beds". In: *The American Naturalist* 165.3, E66–E77. ISSN: 0003-0147. DOI: 10.1086/428362. URL: http://www.journals.uchicago.edu/doi/10.1086/428362.

LeVeque, Randall J (2007). *Finite difference methods for ordinary and partial differential equations: steady-state and time-dependent problems*. Vol. 98. Siam.

Macfadyen, W. A. (1950). "Vegetation patterns in the semi-desert plains of British Somaliland". In: *Geographical Journal* 116.4/6, pp. 199–211. ISSN: 00167398, 14754959. DOI: 10.2307/1789384. URL: https://www.jstor.org/stable/1789384?origin=crossref.

Medeiros, Stephen C. and Scott C. Hagen (2012). "Review of wetting and drying algorithms for numerical tidal flow models". In: *International Journal For Numerical Methods in Fluids* 71, pp. 473–487. DOI: 10.1002/fld.3668.

Meijer, Hil, Fabio Dercole, and Bart Oldeman (2009). "Numerical bifurcation analysis". In: *Encyclopedia of Complexity and Systems Science*. Springer, pp. 6329–6352.

Ranasinghe, Roshanka et al. (2011). "Morphodynamic upscaling with the MORFAC approach: Dependencies and sensitivities". In: *Coastal Engineering* 58.8, pp. 806–811. ISSN: 03783839. DOI: 10.1016/j.coastaleng.2011.03.010. URL: http://dx.doi.org/10.1016/j.coastaleng.2011.03.010.

Renshaw, E. and E. D. Ford (1984). "The description of spatial pattern using two-dimensional spectral analysis". In: *Vegetatio* 56.2, pp. 75–85. ISSN: 00423106. DOI: 10.1007/BF00033049.

Rietkerk, Max and Johan van de Koppel (2008). "Regular pattern formation in real ecosystems". In: *Trends in Ecology and Evolution* 23.3, pp. 169–175. ISSN: 01695347. DOI: 10.1016/j.tree.2007.10.013. URL: http://linkinghub.elsevier.com/retrieve/pii/S0169534708000281.

Rietkerk, Max et al. (2002). "Self-Organization of Vegetation in Arid Ecosystems". In: *The American Naturalist* 160.4, pp. 524–530. ISSN: 0003-0147. DOI: 10.1086/342078. URL: http://www.journals.uchicago.edu/doi/10.1086/342078.

Rietkerk, Max et al. (2004). "Self-organized patchiness and catastrophic shifts in ecosystems". In: *Science* 305.5692, pp. 1926–1929. ISSN: 00368075. DOI: 10.1126/science.1101867. URL: http://www.sciencemag.org/cgi/doi/10.1126/science.1101867.

Saco, P. M., G. R. Willgoose, and G. R. Hancock (2007). "Eco-geomorphology of banded vegetation patterns in arid and semi-arid regions". In: *Hydrology and Earth System Sciences* 11.6, pp. 1717–1730. ISSN: 16077938. DOI: 10.5194/hess-11-1717-2007.

Saco, Patricia M. and Mariano Moreno-De Las Heras (2013). "Ecogeomorphic coevolution of semiarid hillslopes: Emergence of banded and striped vegetation patterns through interaction of biotic and abiotic processes". In: *Water Resources Research* 49.1, pp. 115–126. ISSN: 00431397. DOI: 10.1029/2012WR012001.

Scheffer, Marten et al. (2001). "Catastrophic shifts in ecosystems". In: *Nature* 413.6856, pp. 591–596. ISSN: 00280836. DOI: 10.1038/35098000.

Segel, Lee A and Marshall Slemrod (1989). "The quasi-steady-state assumption: a case study in perturbation". In: *SIAM review* 31.3, pp. 446–477.

Sherratt, Jonathan A. (2015). "Using wavelength and slope to infer the historical origin of semiarid vegetation bands". In: *Proceedings of the National Academy of Sciences* 112.14, pp. 4202–4207. ISSN: 0027-8424. DOI: 10.1073/pnas.1420171112. URL: http://www.pnas.org/lookup/doi/10.1073/pnas.1420171112.

Simpson, Guy and Sébastien Castelltort (2006). "Coupled model of surface water flow, sediment transport and morphological evolution". In: *Computers and Geosciences* 32.10, pp. 1600–1614. ISSN: 00983004. DOI: 10.1016/j.cageo.2006.02.020. URL: http://linkinghub.elsevier.com/retrieve/pii/S0098300406000458.

Siteur, Koen et al. (2014). "Beyond Turing: The response of patterned ecosystems to environmental change". In: *Ecological Complexity* 20, pp. 81–96. ISSN: 1476945X. DOI: 10.1016/j.ecocom.2014.09.002. URL: http://dx.doi.org/10.1016/j.ecocom.2014.09.002.

Varberg, Dale E, Edwin Joseph Purcell, and Steven E Rigdon (2007). *Calculus with differential equations*. Pearson/Prentice Hall.

Veldman, AEP (2001). "Computational fluid dynamics". In: *Lecture Notes, University of Groningen, The Netherlands*.

Weerman, Ellen J. et al. (2010). "Spatial Self-Organization on Intertidal Mudflats through Biophysical Stress Divergence". In: *The American Naturalist* 176.1, E15–E32. ISSN: 0003-0147. DOI: 10.1086/652991. URL: http://www.journals.uchicago.edu/doi/10.1086/652991.

Weisstein, Eric W (2018). *Courant-Friedrichs-Lewy Condition*. URL: http://mathworld.wolfram.com/Courant-Friedrichs-LewyCondition.html (visited on 12/14/2018).